JGS
Journal of the Geological Society

Research article

https://doi.org/10.1144/jgs2020-199 | Vol. 178 | 2021 | jgs2020-199

Segmentation of the Caledonian orogenic infrastructure and exhumation of the Western Gneiss Region during transtensional collapse

J.D. Wiest[1*], J. Jacobs[1], H. Fossen[1,2], M. Ganerød[3] and P.T. Osmundsen[4,5]

[1] Department of Earth Science, University of Bergen, PB 7803, 5020 Bergen, Norway
[2] Museum of Natural History, University of Bergen, PB 7803, 5020 Bergen, Norway
[3] Norwegian Geological Survey, PB 6315, 7491 Trondheim, Norway
[4] Department of Geoscience and Petroleum, Norwegian University of Science and Technology, Sem Sælandsvei 1, 7491 Trondheim, Norway
[5] Department of Geosciences, University of Oslo, 0316 Oslo, Norway
JDW, 0000-0002-5343-9194; MG, 0000-0003-0051-4020
* Correspondence: johannes.wiest@uib.no

Abstract: The (ultra)high-pressure Western Gneiss Region of the Norwegian Caledonides represents an archetypical orogenic infrastructure of a continent–continent collision zone. To test established exhumation models, we synthesize the geochronology and structures of major basement windows and provide new ages from poorly dated areas. Migmatite U–Pb zircon samples date melt crystallization at *c.* 405 Ma in the Øygarden Complex, expanding the spatial extent of Devonian migmatization. Micas from shear zones in the Øygarden and Gulen domes yield $^{40}Ar/^{39}Ar$ ages mostly between 405 and 398 Ma, recording the exhumation of metamorphic core complexes. On a larger scale, the youngest ages of various geochronometers in different segments of the Western Gneiss Region show abrupt breaks (10–30 myr) across low-angle detachments and sinistral transfer zones, which also correspond to metamorphic and structural discontinuities. We explain the segmentation of the orogenic infrastructure by partitioned post-orogenic transtension due to lateral and vertical rheological contrasts in the orogenic edifice (strong cratonic foreland and orogenic wedge v. soft infrastructure). Differential crustal stretching dragged out deep levels of the orogenic crust below low-angle detachments and became progressively dominated by sinistral transfer zones. Collapse obliterated the syn-collisional structure of the orogenic root and resulted in the diachronous exhumation of distinct infrastructure segments.

Supplementary material: Complete analytical results are available at https://doi.org/10.6084/m9.figshare.c.5241710

Received 22 October 2020; **revised** 8 December 2020; **accepted** 15 December 2020

Large areas of West Norway consist of gneiss and are conveniently called the Western Gneiss Region (WGR). The WGR comprises the part of the ancient margin of Baltica that was subducted during the Silurian–Devonian Caledonian orogeny (Fig. 1; Gee *et al.* 2008). Today, it represents one of the Earth's largest, best exposed and most studied (ultra)high-pressure ((U)HP) terranes (Wain 1997; Hacker *et al.* 2010). As such, it is crucial for our understanding of (deep) orogen dynamics (Vanderhaeghe 2012), the extensional collapse of overthickened crust (Rey *et al.* 2001), the formation and exhumation of (U)HP rocks (Warren 2013) and structural inheritance affecting later tectonic episodes (Peron-Pinvidic and Osmundsen 2020).

The geodynamic evolution from Caledonian continental collision (Corfu *et al.* 2014; Torsvik 2019) to post-orogenic collapse (Fossen 2010) and the event chronology from (U)HP metamorphism to retrograde reworking (e.g. Hacker *et al.* 2010; Kylander-Clark and Hacker 2014; Butler *et al.* 2018) are generally well constrained and validated by 2D numerical models (Duretz *et al.* 2012; Butler *et al.* 2015). Widely accepted tectonic models (Fig. 1) postulate the exhumation of the WGR as a coherent crustal slab (e.g. Hacker *et al.* 2010; Kylander-Clark and Hacker 2014). However, these models are limited to two dimensions and neglect the 3D structural complexity inherent in the WGR (e.g. Fossen *et al.* 2013). Furthermore, some of these models invoke that the WGR was exhumed as a rigid block above a syn-exhumation thrust, for which there is no field or geophysical evidence (Fig. 1). Although geochronological discrepancies between different parts of the WGR have been noted previously (Labrousse *et al.* 2004), they are not adequately integrated into tectonic models and are concealed by the lack of data from marginal parts of the WGR.

The aim of this paper is to develop a more realistic exhumation model that reconciles the structural and geochronological record of the entire WGR with the 3D transtensional boundary conditions of orogenic collapse (Krabbendam and Dewey 1998; Osmundsen *et al.* 2006; Fossen *et al.* 2013). To do this, we provide a geochronological and structural synthesis of basement windows in a >600 km wide portion of the Norwegian Caledonides (Fig. 2). In addition, we dated migmatites (secondary ion mass spectrometry (SIMS) U–Pb zircon) and shear zones ($^{40}Ar/^{39}Ar$ mica) in the previously poorly constrained southernmost windows. We point out major chronological, structural and metamorphic discontinuities in the former orogenic infrastructure and discuss their relation with major shear zones. This allows us to refine the tectonic models of post-orogenic collapse and its effect on the lithospheric structure before and after orogeny.

Geological setting

The Baltic Shield in West Norway originally formed between 1.8 and 1.5 Ga (Roberts and Slagstad 2015) and its crustal architecture was largely arranged during the 1.2–0.9 Ga Sveconorwegian period (Bingen *et al.* 2005). The latter consisted of multiple orogenic

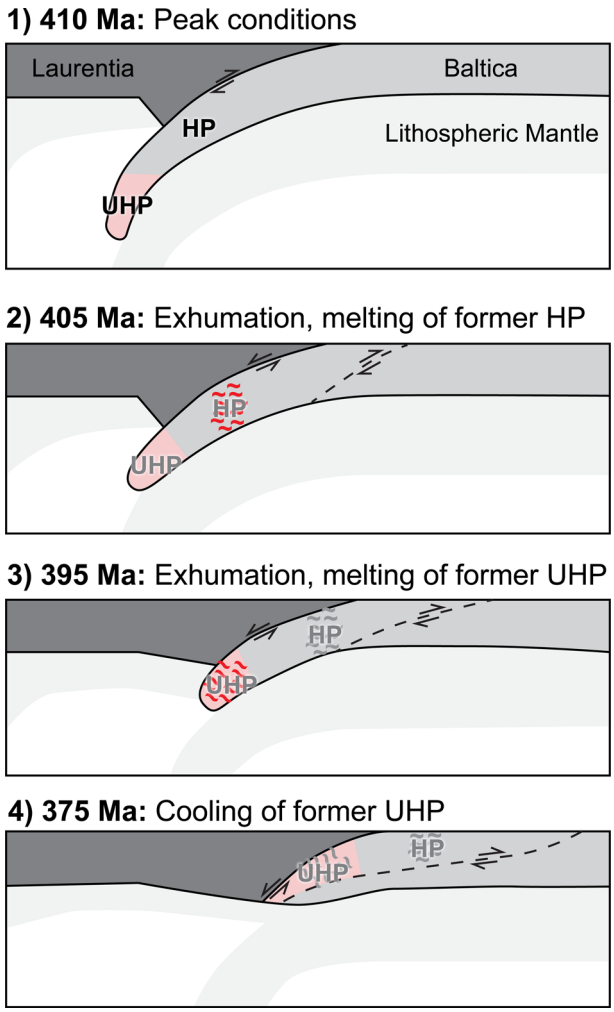

Fig. 1. Previous exhumation models of the Western Gneiss Region (redrawn from Kylander-Clark and Hacker 2014) invoke a syn-exhumation thrust at the base, for which there is no evidence. HP, high-pressure domain; UHP, ultra-high-pressure domain.

phases (Bingen *et al.* 2008), voluminous magmatism (Coint *et al.* 2015; Wiest *et al.* 2018) and widespread migmatization (Slagstad *et al.* 2013, 2018). Subsequent opening of the Iapetus Ocean formed a passive margin (Andersen *et al.* 2012; Jakob *et al.* 2019; Kjøll *et al.* 2019) and led to the deposition of Cambrian shales onto the deeply eroded and transgressed Baltic Shield (Gee *et al.* 2008). The Caledonian orogeny evolved related to the closure of the Iapetus Ocean and culminated in the Silurian–Devonian (Scandian) collision between Baltica, Avalonia and Laurentia (Roberts 2003; Corfu *et al.* 2014). Different units originating from the Iapetus Ocean, the Laurentian margin and the Baltican margin were thrust towards the SE onto the Baltic Shield (present orientation). Cambrian shales provided a weak basal décollement that allowed stacking of a thick, but relatively cold, orogenic wedge (Fossen 1992; Fauconnier *et al.* 2014; Fossen *et al.* 2017), whereas the Baltican margin was subducted to mantle depths below Laurentia (Griffin and Brueckner 1980; Brueckner 2018). The break-off of the oceanic slab and/or the northwards indentation of Avalonia (Rey *et al.* 1997; Fossen 2010) led to extensional collapse of the Caledonian orogen from *c.* 410 Ma (Fossen and Dunlap 1998). First, slab eduction (Andersen *et al.* 1991) led to the reversal of the basal décollement and pervasive hinterland-directed shearing in the ductile lower parts of the nappe pile (Fossen 1992, 1993, 2000; Osmundsen and Andersen 1994). Soon after, wholesale crustal collapse formed an orogen-wide detachment system (McClay *et al.* 1986; Norton 1986; Andersen and Jamtveit 1990; Milnes and Koyi 2000; Fossen and Hurich 2005; Fossen 2010; Duretz *et al.* 2012). Sinistral transtension led to coaxial stretching of the deep crust, crustal-scale necking, constrictional folding and the formation of strongly corrugated detachments and strike-slip transfer zones (Figs 2 and 3) (Andersen *et al.* 1994; Chauvet and Seranne 1994; Krabbendam and Dewey 1998; Osmundsen and Andersen 2001; Dewey 2002; Labrousse *et al.* 2002; Dewey and Strachan 2003; Osmundsen *et al.* 2006; Hacker *et al.* 2010; Fossen *et al.* 2013). Metamorphic core complexes (MCCs) exhumed deep crust from the orogenic root, which was juxtaposed with Devonian supra-detachment basins (Hossack 1984; Séguret *et al.* 1989; Braathen *et al.* 2000; Eide *et al.* 2005; Osmundsen *et al.* 2005; Braathen *et al.* 2018; Wiest *et al.* 2019; Wiest *et al.* 2020*a*). Permian to Mesozoic North Sea rifting brittlely overprinted and partly reactivated collapse structures (Eide *et al.* 1997; Andersen *et al.* 1999; Fossen *et al.* 2016).

Structure and geochonology of the WGR

Different terminologies are used for the Baltican basement windows of Western Norway. Here, we distinguish three first-order entities, which, for simplicity, we call the Northern, Central and Southern WGR (Fig. 2a). The Møre–Trøndelag Fault Zone separates the Northern WGR and Central WGR, whereas the Nordfjord and Lom Shear Zones delimit the Southern WGR close to 62° N. The Øygarden Complex is the southernmost window and is separated from the Southern WGR by allochthons in the Bergen Arcs. However, it is similar to second-order domes inside the Southern WGR, such as the Gulen dome. The basement windows show similar structural architectures (Fig. 3), but their widths range from *c.* 50 km in the south (Fig. 3, section E–E′) to *c.* 150 km in the Northern WGR (Fig. 3, section B–B′) and *c.* 200 km in the Central WGR (Fig. 3, section C–C′). Based on a newly compiled geochronological database (Supplementary Material ES-2), we describe the structures and ages of different parts of the WGR.

Northern WGR

The Northern WGR (also referred to as the Vestranden Gneiss Complex or Central Norway Basement Window) consists of 1.8–1.6 Ga Baltic Shield basement, unaffected by the Sveconorwegian orogeny, and infolded allochthons (Schouenborg *et al.* 1991; Johansson *et al.* 1993; Gordon *et al.* 2016). North of the Møre–Trøndelag Fault Complex (Fig. 2a), the Northern WGR represents a bivergent MCC (Fig. 3, section B–B′) that was exhumed by the Høybakken (top-to-the-SW) and the Kollstraumen (top-to-the-NE) detachments (Dallmeyer *et al.* 1992; Braathen *et al.* 2000; Kendrick *et al.* 2004; Gordon *et al.* 2016). Internal subdomes contain migmatites, granulites and high-pressure eclogites (UHP indicators are absent), whereas allochthons are folded around the domes into pinched synclines (Fig. 2b). Migmatites in the nappes are 430 Ma or older, whereas Scandian leucosomes (410–405 Ma) have been dated in domes in the footwall of the Høybakken Detachment (Gordon *et al.* 2016). $^{40}Ar/^{39}Ar$ ages from the nappes are ≥420 Ma (Dallmeyer 1990), mostly 400–390 Ma inside the Northern WGR (Dallmeyer *et al.* 1992) and as young as 382 Ma in the Høybakken Detachment (Kendrick *et al.* 2004). Detrital ages from sandstones and conglomerates in the overlying Devonian basins suggest that the Northern WGR was exhumed and eroded during Late Devonian to Early Carboniferous basin deposition (Eide *et al.* 2005).

Central WGR

The Central WGR consists of *c.* 1.6 Ga Baltic Shield with a strong Sveconorwegian imprint in the SW, but diminishing effects towards

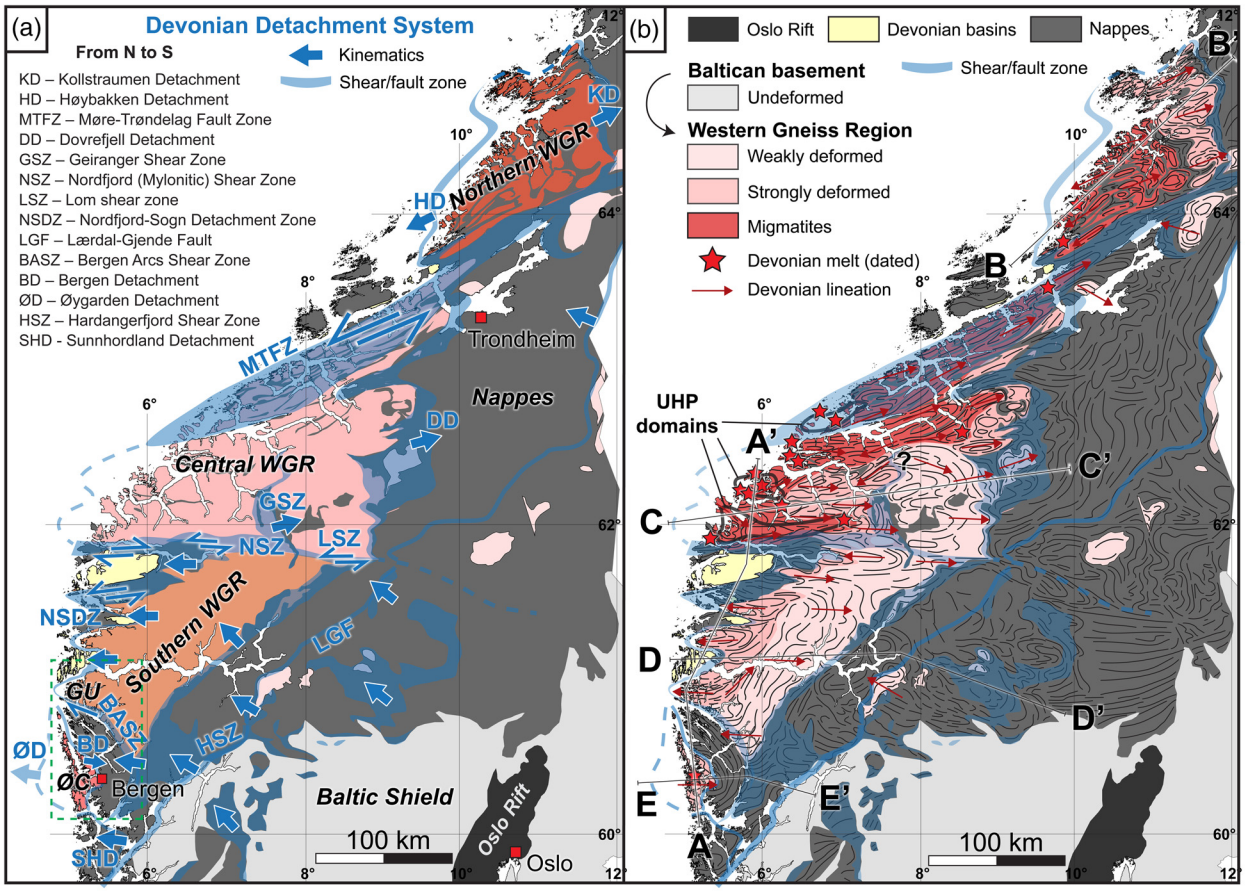

Fig. 2. Tectonic maps of basement windows in the Caledonides of Western Norway. (**a**) Structures and kinematics of the Devonian detachment system and terminology used for the basement windows. We distinguish three domains (Northern, Central and Southern) of the Western Gneiss Region. The Gulen metamorphic core complex and Øygarden Complex represent second-order domes. (**b**) The Western Gneiss Region consists of Baltican basement in different deformation states (the extent of partial melting is poorly constrained). Foliation traces (shapefiles in Supplementary Material ES-1) have been mapped based on the digital structural database of the Norwegian Geological Survey. Note how the foliation traces in the strongly deformed basement mostly align with Devonian stretching lineations. Locations of the cross-sections in Fig. 3 are marked as A–A′, B–B′, C–C′, D–D′ and E–E′. GU, Gulen metamorphic core complex; ØC, Øygarden Complex; UHP, ultra-high-pressure.

the NE (Tucker *et al.* 1987; 1990; Røhr *et al.* 2013). The Baltican crust (also termed the Western Gneiss Complex) hosts variably overlying or infolded allochthons (Robinson *et al.* 2014; Hacker *et al.* 2015; Walczak *et al.* 2019) and externally derived mantle rocks (Brueckner 2018). The gneissic tectonites show increasing strain from SE to NW (Hacker *et al.* 2010), corresponding to deeper levels of an east-dipping homocline (Fig. 3, section C–C′).

The UHP rocks define three distinct domains (Fig. 2B; together *c.* 5000 km^2), which can be interpreted as upright mega-folds (Fig. 3, section A–A′), surrounded by *c.* 30 000 km^2 of high-pressure rocks (Cuthbert *et al.* 2000; Root *et al.* 2005; Hacker *et al.* 2010). The northern boundary of the Central WGR, the Møre–Trøndelag Shear/Fault Zone (Fig. 2a), represents a sinistral transfer zone between the SW-directed Høybakken Detachment and the Nordfjord–Sogn Detachment Zone (Krabbendam and Dewey 1998; Braathen *et al.* 2000). The boundary to the Southern WGR is the east–west-striking sinistral Nordfjord Shear Zone (Labrousse *et al.* 2004). In its eastern continuation, reconnaissance mapping has identified the Lom Shear Zone (Supplementary Material ES-3) as a major sinistral shear zone (Fig. 2a). Geographically, the Nordfjord–Lom Shear Zones coincide with the eclogite-in isograd and the 600°C isotherm of Hacker *et al.* (2010). Towards the coast, the sinistral Nordfjord Shear Zone becomes overprinted by the Sandane (top-to-the west) shear zone and the dextral Hornelen Detachment, which are both part of the Nordfjord–Sogn Detachment Zone (Labrousse *et al.* 2004; Johnston *et al.* 2007*a*; Young *et al.* 2011).

The eastern boundary of the Central WGR is an ENE-directed shear zone with complex structural relationships (here termed the Dovrefjell Detachment; Fig. 2a). The geochronological, structural and metamorphic break between the WGR in the footwall and nappes in the hanging wall (Krill 1985; Hacker and Gans 2005; Hacker *et al.* 2010; Robinson *et al.* 2014) suggests that extensional detachment shearing reactivated an earlier thrust. Along-strike, the footwall shows large structural variations together with increasing strain from south to north (Fig. 2b). In the south, the sinistral strike-slip Lom Shear Zone is cut by low-angle, ductile-to-brittle top-to-the-east shear zones with identically oriented stretching lineations (Supplementary Material ES-3). Towards the north, thrust-related imbrication structures (Robinson *et al.* 2014) were overprinted by rising gneiss domes, which folded the allochthons into cascading folds and pinched synclines (Krill 1985). Towards the north, sinistral shearing related to the Møre–Trøndelag Shear/Fault Zone overprinted earlier top-to-the-WSW shearing (Seranne 1992; Robinson 1995; Osmundsen *et al.* 2006). Located inside the Central WGR, the east-dipping, top-to-the-east Geiranger Shear Zone (Young 2017) separates strongly deformed rocks and UHP assemblages in the footwall from weakly deformed gneisses with high-pressure eclogites in the hanging wall (Fig. 3, section C–C′). Although Young (2017) interpreted this shear zone as a thrust related to the internal imbrication of the WGR, several arguments point towards an extensional origin for this structure.

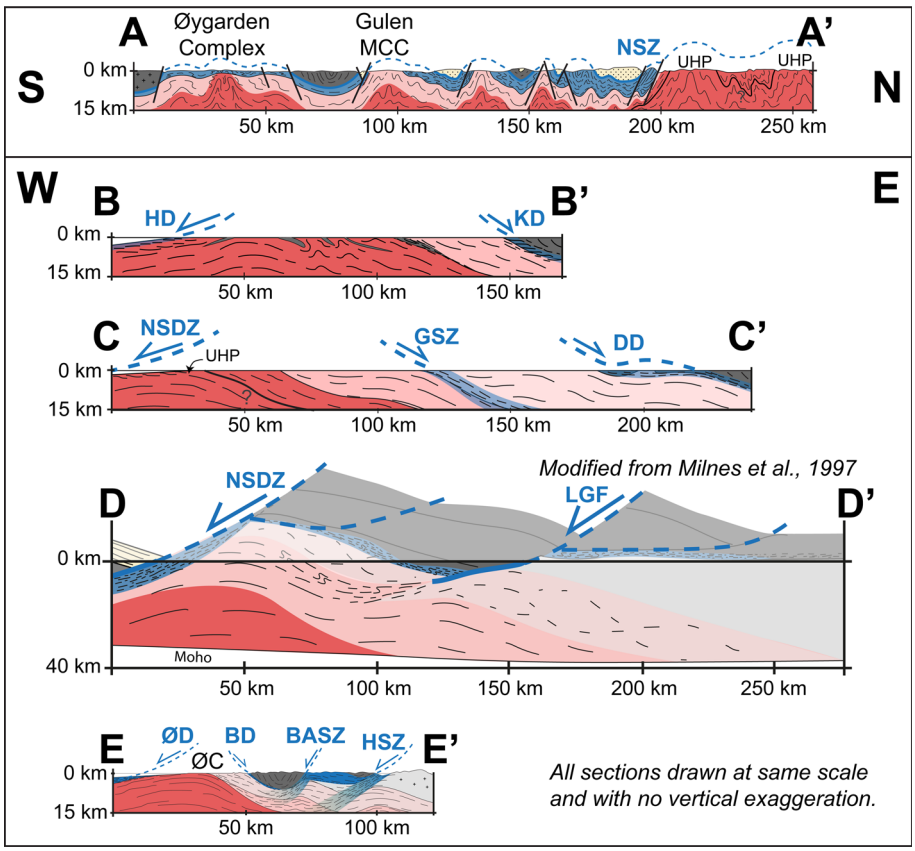

Fig. 3. Extension-perpendicular (A–A′) and extension-parallel (B–B′, C–C′, D–D′ and E–E′) cross-sections of basement windows showing structural similarities, but variable sizes. Based on: (A–A′) Krabbendam and Dewey (1998), Johnston *et al.* (2007*b*) and Wiest *et al.* (2019); (B–B′) Braathen *et al.* (2002); (C–C′) Hacker *et al.* (2010) and Young (2017); (D–D′) Milnes *et al.* (1997); and (E–E′) Wiest *et al.* (2020*a*) and Fossen and Hurich (2005). Abbreviations as in Figure 2a and locations shown in Figure 2b.

A large number of studies have addressed the temporal evolution of the Central WGR, particularly focusing on the UHP domains. Eclogite age determinations (Lu–Hf and Sm–Nd garnet, U–Pb zircon and monazite) range mostly from 420 to 400 Ma, with a probability peak at *c.* 410 Ma (see compilation by Kylander-Clark and Hacker 2014). The overlap of eclogite ages (Krogh *et al.* 2011) and leucosome U–Pb zircon ages (405–390 Ma) fuelled debate about whether melting started at (U)HPs and facilitated exhumation (Labrousse *et al.* 2002, 2011; Gordon *et al.* 2013) or whether melting resulted from decompression (Kylander-Clark and Hacker 2014; Butler *et al.* 2015; Kohn *et al.* 2015). The U–Pb titanite ages of felsic gneisses range from 410 to 380 Ma (except for partially reset grains), with the bulk of ages between 400 and 390 Ma (Spencer *et al.* 2013). U–Pb monazite (Hacker *et al.* 2015) and U–Pb rutile ages show a similar distribution, the latter including ages ≤380 Ma from eclogites (Kylander-Clark *et al.* 2008; Butler *et al.* 2018; Cutts *et al.* 2019). Most $^{40}Ar/^{39}Ar$ ages (mostly white mica) in the Central WGR are *c.* 400–375 Ma, generally becoming younger from SE to NW (Walsh *et al.* 2007, 2013; Young *et al.* 2011). The nappes in the east have $^{40}Ar/^{39}Ar$ ages commonly older than 415 Ma (Hacker and Gans 2005), but allochthons within the WGR show similar $^{40}Ar/^{39}Ar$ ages to the basement gneisses (≤400 Ma). Systematic studies suggest that $^{40}Ar/^{39}Ar$ mica ages variably record the effects of metamorphism, fluids and deformation and cannot be reconciled with simple cooling through a temperature window (e.g. Warren *et al.* 2012; McDonald *et al.* 2016). Detrital data from the Hornelen basin include Devonian U–Pb zircon and $^{40}Ar/^{39}Ar$ ages consistent with previous interpretations that parts of the Central WGR and/or the detachment zones were exhumed and eroded during basin formation (Templeton 2015).

Southern WGR

The Southern WGR consists mostly of *c.* 1.6 Ga Baltic Shield with widespread evidence of Sveconorwegian magmatism and migmatization (Skår and Pedersen 2003; Røhr *et al.* 2004, 2013). Although the Baltican basement is generally weakly deformed (Fig. 2b), strongly deformed eclogite-bearing crust forms three footwall domes below the Nordfjord–Sogn Detachment Zone (Norton 1987; Andersen *et al.* 1994; Milnes *et al.* 1997; Krabbendam and Dewey 1998; Johnston *et al.* 2007*b*; Wiest *et al.* 2019). The domes in the footwall of the strongly corrugated detachment have a similar wavelength to the mega-folds in the Central WGR (Fig. 3, section A–A′). Synforms in the hanging wall of the detachment are occupied by scoop-shaped Devonian basins (Hossack 1984; Seranne and Séguret 1987; Osmundsen and Andersen 2001; Vetti and Fossen 2012) and various allochthons (Osmundsen and Andersen 1994; Hacker *et al.* 2003). The latter commonly show $^{40}Ar/^{39}Ar$ ages older than *c.* 410 Ma (Andersen *et al.* 1998; Fossen and Dunlap 2006). The nappes inside the detachment zones, by contrast, have similar $^{40}Ar/^{39}Ar$ ages to the basement in the underlying MCCs (*c.* 410–400 Ma), whereas younger ages are found in the WGR away from the detachments (*c.* 400–395 Ma; Chauvet and Dallmeyer 1992; Boundy *et al.* 1996; Fossen and Dunlap 1998; Walsh *et al.* 2013). Labrousse *et al.* (2004) noted a significant age difference across the Nordfjord Mylonitic Shear Zone and suggested that the Southern and the Central WGR represent distinct levels of the orogenic wedge with contrasting *P–T–t* and deformation histories.

Gulen MCC

The Gulen MCC represents the southernmost culmination of the WGR (Fig. 2a) and marks the southern limit of high-pressure metamorphism in the Baltic Shield (Wiest *et al.* 2019). To the north, the Nordfjord–Sogn Detachment Zone separates the Gulen dome from the Solund basin (Osmundsen and Andersen 2001; Hartz *et al.* 2002; Hacker *et al.* 2003; Braathen *et al.* 2004; Souche *et al.* 2012), while the Bergen Arcs Shear Zone juxtaposes its southern flank against small remnants of the Fensfjorden Devonian basin

(Wennberg *et al.* 1998). Covering an area of 40 km × 30 km, the Gulen dome has a gradual transition into less deformed basement towards the east (Fig. 4) and continues underneath the North Sea basin towards the west (Wiest *et al.* 2020*b*). The dome consists of two distinct domains (Wiest *et al.* 2019). The core preserves amphibolite facies fabrics in coaxial subvertical shear zones with metre- to kilometre-scale tight upright folds parallel to sub-horizontal east–west-trending stretching lineations. Eclogites hosted inside the gneissic shear zones show evidence of fluid-induced retrogression. Wrapping around the core, detachment mylonites are distinguished by top-to-the-west shearing, vertical shortening and retrograde deformation down to semi-brittle conditions. Wiest *et al.* (2019) explain dome formation through the deep crustal, extension-perpendicular, inward flow of low-viscosity solid-state material in response to detachment faulting thinning the upper crust. Apart from Sveconorwegian U–Pb zircon and monazite ages (Røhr *et al.* 2004), no previous geochronological data is available from the Gulen dome.

Øygarden Complex

The Øygarden Complex is a dome-shaped window consisting of Telemarkian (1.5 Ga) and Sveconorwegian (1.0 Ga) Baltic Shield basement (Wiest *et al.* 2018). The dome forms the core of the Bergen Arcs megastructure (Fig. 4), which is made of various nappes folded into an arc-shaped synform (Kolderup and Kolderup 1940). The Øygarden Complex represents a bivergent MCC (Wiest *et al.* 2020*a*) with a major west-directed detachment located offshore (Øygarden Detachment; Figs 2 and 3, section E–E′) and an antithetic east-directed detachment (Bergen Detachment) that reactivated the basal thrust in the Bergen Arcs (Fossen 1989). To the north, the Øygarden Complex is overlain by small remnants of Devonian supra-detachment basins, whereas its southern flank is juxtaposed against the Sunnhordland nappe (Andersen and Jansen 1987). In contrast with the Gulen MCC, there are no eclogites and the entire Øygarden dome shows ductile-to-brittle deformation characteristic of the detachment domain. Three distinct structural levels are characterized (from top to bottom) by localized shear, distributed ductile flow and a migmatite dome at the lowest level of the complex (Wiest *et al.* 2020*a*). All the structural levels record east–west stretching with similar fabric orientations and retrogressive overprinting, but with opposed kinematics at the upper (top-to-the-east) and middle–lower levels (top-to-the-west). Wiest *et al.* (2020*a*) suggest that extension-perpendicular flow of the partially molten deep crust formed a dome, whereas retrogressive fabric weakening facilitated bivergent detachment formation. The few available $^{40}Ar/^{39}Ar$ biotite and hornblende ages range between 408 and 401 Ma (Boundy *et al.* 1996; Fossen and Dunlap 1998) and the

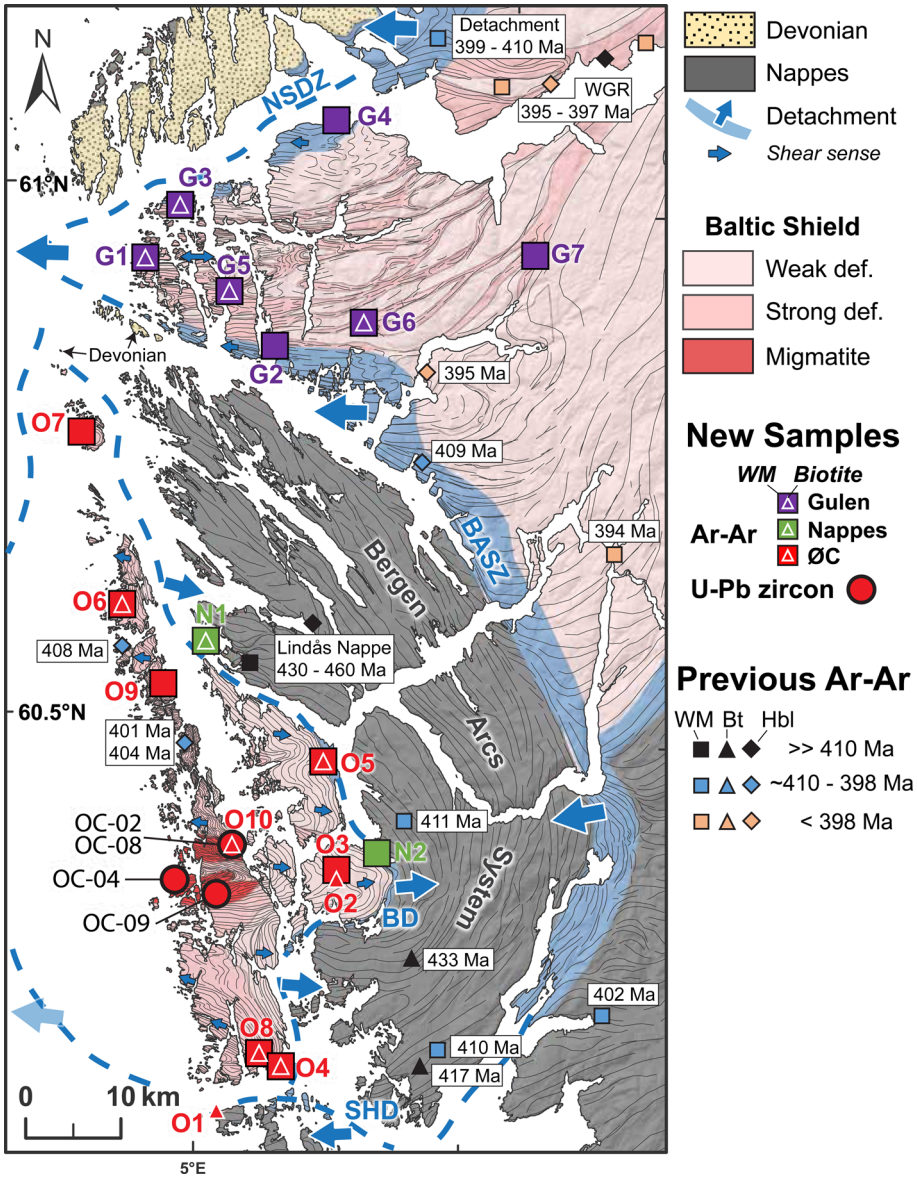

Fig. 4. Tectonic map of the Gulen metamorphic core complex and Øygarden Complex (based on Wiest *et al.* 2019, 2020*a*) showing new geochronology samples from this study and previously published $^{40}Ar/^{39}Ar$ ages. BASZ, Bergen Arcs Shear Zone; BD, Bergen Detachment; Bt, biotite; Hbl, hornblende; NSDZ, Nordfjord–Sogn Detachment Zone; ØC, Øygarden Complex; SHD, Sunnhordland Detachment; WM, white mica.

U–Pb dating of titanite in fractures constrains the onset of brittle faulting to *c.* 396 Ma (Larsen *et al.* 2003). Coast-parallel fractures host Permian–Triassic alkaline dykes (Fossen and Dunlap 1999), whereas K/Ar illite fault gouge dating indicates repeated fault reactivation from the Carboniferous to the Cretaceous (Ksienzyk *et al.* 2014, 2016; Fossen *et al.* 2016).

Samples and methods

To test the significance of the age discrepancy between different parts of the WGR, we collected leucosome samples for SIMS U–Pb zircon dating of migmatites in the Øygarden Complex and samples of gneisses and schists from 19 shear zones in the Gulen MCC, the Øygarden Complex and nappes in the Bergen Detachment for $^{40}Ar/^{39}Ar$ mica dating (Fig. 4; Table 1). While aiming at white mica (16 samples), we also present 12 complementary biotite ages for samples where both micas were present or for shear zones where no white mica could be obtained. Additional documentation for all new samples is provided in the electronic Supplementary Material ES-4.

SIMS U–Pb zircon geochronology

We collected four granitic leucosomes from migmatites in the core of the Øygarden Complex (Fig. 4). The leucosomes were crushed and the separated zircon grains were hand-picked, mounted in epoxy, polished and imaged by cathodoluminescence. U–Pb geochronology was performed using a CAMECA IMS1280 large-geometry ion microprobe at the Nordsim Laboratory, Stockholm, following routine procedures outlined by Whitehouse *et al.* (1999) and Whitehouse and Kamber (2005). Using a spot diameter of *c.* 10 µm, groups of analyses were performed in fully automated sequences, regularly interspersing reference material analyses with those of the sample zircon grains. Data reduction used a suite of software developed in-house. Pb isotope ratios were corrected for common Pb estimated from measured ^{204}Pb assuming the present day terrestrial Pb isotope composition (assuming common Pb is a modern surface contamination) calculated with the model of Stacey and Kramers (1975), except where the ^{204}Pb count was statistically insignificant. U/Pb ratios were calibrated using a Pb/UO–UO_2/UO calibration (Jeon and Whitehouse 2015) from regular measurements of the 1065 Ma 91500 zircon (Wiedenbeck *et al.* 1995). The age calculations assume the decay constant recommendations of Steiger and Jäger (1977) and use the routines of Isoplot-Ex (Ludwig 2003). All age uncertainties include uncertainties on the decay constants as well as propagation of the error on the Pb/UO–UO_2/UO calibration (Whitehouse *et al.* 1997; Jeon and Whitehouse 2015) and are reported at 2σ if not specified otherwise. For concordia ages, the mean square of weighted deviates (MSWD) on combined equivalence and concordance is reported following the recommendation of Ludwig (1998). Concordia diagrams and representative zircon images are shown in Figure 5, whereas the analytical results can be found in Supplementary Material ES-6.

$^{40}Ar/^{39}Ar$ mica dating

We collected seven samples in the Gulen MCC from different domains described by Wiest *et al.* (2019): three samples from the detachment zone (G1, G2 and G4); two from a transitional domain (G3 and G6); sample G5 from the core; and sample G7 from a shear zone east of the dome itself (Fig. 4). Two samples from the Caledonian nappes overlaying the Øygarden Complex represent the Bergen Detachment (N1 and N2). We collected samples in the Øygarden Complex from shear zones described in detail by Wiest *et al.* (2020*a*). Two samples represent the bounding shear–fault zones of the complex (O1 and O5). We sampled three top-to-the-east shear zones from the upper (eastern) unit (O2, O3 and O4) and four top-to-the-west shear zones from the middle unit (O6, O7, O8 and O9). Sample O10 represents the migmatite domain at the lowest level of the Øygarden Complex.

Where possible, we extracted white mica and biotite from each sample and hand-picked the optically best grains for $^{40}Ar/^{39}Ar$ incremental heating experiments performed at the Norwegian Geological Survey, Trondheim. We present 16 white mica and 12 biotite plateau ages calculated from $^{40}Ar/^{39}Ar$ incremental release spectra (Figs 6–8, Supplementary Material ES-4). Analytical procedures and age/error calculations are described in detail in Supplementary Material ES-5. We define a plateau according to the following requirements: at least three consecutive steps overlapping at the 95% confidence level (1.96σ), ≥50% cumulative ^{39}Ar released and MSWD less than the two-tailed Student's *T* critical test statistics for $(n-1)$. Uncertainties are reported at the 95% confidence level and complete analytical results are documented in Supplementary Material ES-6.

Geochronology results

SIMS U–Pb zircon dating of migmatites in the Øygarden Complex

OC-02

Sample OC-02 is a granitic stromatic metatexite with folded hornblende-bearing leucosomes (Supplementary Material ES-4) collected in the village of Spjeld. The leucosomes are surrounded by melanosomes, form schlieren and are usually centimetres wide, but melt was also collected in decimetre-thick veins. Although the leucosomes have magmatic microtextures, the biotite melanosomes show an east-plunging mineral stretching lineation related to weak localized shearing. The sampled leucosomes contain two zircon populations with distinct optical characteristics, morphologies and chemical compositions. The first population consists of intermediate size (100–200 µm), yellowish brown, euhedral to rounded zircons, which commonly show multiple growth domains in cathodoluminescence images. They consist of angular cores with simple zoning surrounded by oscillatory or sector-zoned domains. The second population consists of similarly sized, colourless, transparent, inclusion-free zircons. Although most grains are euhedral, sometimes with slightly rounded corners, soccer ball morphologies are also observed. Most grains have xenocrystic cores consisting of the first described zircon population. The cores are partly resorbed and surrounded by oscillatory or sector-zoned domains. Other grains have no core and show simple, oscillatory or fir tree zoning (Fig. 5), which is a typical feature of granulite facies zircon (Vavra *et al.* 1996).

The 53 analysed spots show variable results conforming with the described zircon populations. The first population yields *c.* 100–2000 ppm U and Th/U ratios mostly between 0.1 and 1.0. A concordia age of 1501 ± 16 Ma (MSWD 0.35) can be calculated for two concordant analyses of the xenocrystic cores (Fig. 5). From the mantling growth domain, 11 concordant analyses give a $^{206}Pb/^{238}U$ weighted mean age of 1001 ± 13 Ma (MSWD 2.9). The second zircon population is characterized by variable, but mostly very low, U concentrations (4–1000 ppm) and Th/U ratios commonly ≤0.01. The $^{206}Pb/^{238}U$ ages range from 430 to 394 Ma and a concordia age of 404.7 ± 3.4 Ma (MSWD 1.5) can be calculated for 25 concordant analyses (Fig. 5).

OC-08

Sample OC-08 is a granitic metatexite that was collected on the Spjeldsfjellet hill *c.* 1 km away from sample OC-02 to confirm the Caledonian age of migmatization. The folded leucosomes are commonly a few centimetres wide and surrounded by biotite

Table 1 *Summary of geochronology samples*

$^{40}Ar/^{39}Ar$ mica*									
Sample	White mica age (Ma)	±2σ	Biotite age (Ma)	±2σ	Lithology	Unit	Kinematics	Latitude	Longitude
Gulen MCC									
G1	424.4	6.9	418.0	3.5	Mylonitic gneiss	Detachment	Top-to-the-west	60.9339	4.8024
G2	410.4	1.1			Garnet mica schist	Detachment	Top-to-the-west	60.8621	5.0697
G3	404.9	4.0	400.4	3.0	Micaceous gneiss	Transition	Sinistral	60.9861	4.8635
G4	402.0	1.2			Mylonitic quartzite	Detachment	Top-to-the-west	61.0789	5.1622
G5	401.9	2.3	405.8	2.2	Garnet mica schist	Core	Coaxial	60.9101	4.9629
G6	400.5	3.0	418.4	2.1	Garnetiferous mylonite	Transition	Top-to-the-west	60.8865	5.2321
G7	393.4	1.7			Micaceous gneiss	Outside MCC	Coaxial	60.9608	5.5559
Nappes									
N1	431.6	2.0	457.3	2.1	Phyllonitic amphibolite	Detachment	Top-to-the-east	60.5791	4.9689
N2	408.4	2.5			Garnet mica schist	Detachment	Top-to-the-east	60.3876	5.3173
Øygarden Complex									
O1			410.3	3.2	Mylonitic gneiss	Detachment	Top-to-the-west	60.1355	5.0411
O2			412.2	2.2	Chlorite–biotite phyllonite	Upper	Top-to-the-east	60.3619	5.2388
O3	404.7	1.8			Muscovite–quartz phyllonite	Upper	Top-to-the-east	60.3720	5.2409
O4	399.8	2.1	402.8	3.2	Phyllonitic gneiss	Upper	Top-to-the-east	60.1847	5.1524
O5	397.5	2.8	399.4	4.5	Garnet mica schist	Detachment	Top-to-the-east	60.4714	5.2006
O6	403.1	1.5	410.5	2.4	Mylonitic quartzite	Middle	Top-to-the-west	60.6088	4.8009
O7	400.6	4.8			Garnet mica schist	Middle	Top-to-the-NW	60.7693	4.6990
O8	400.5	2.4	401.9	2.5	Phyllonitic gneiss	Middle	Top-to-the-west	60.1914	5.1117
O9	399.5	2.2			Garnet mica schist	Middle	Top-to-the-west	60.5349	4.8904
O10			403.8	1.6	Metatexite melanosome	Lower	Top-to-the-west	60.3876	5.0397
U–Pb zircon: Øygarden Complex									
Sample	Calculated. age (Ma)	±2σ	Sveconorwegian age (Ma)	±2σ	Lithology	Unit	Comment	Latitude	Longitude
OC-02	404.7	3.4	1001	13	Granitic metatexite	Lower	Hornblende leucosome	60.3876	5.0397
OC-04			1001	17	Granodioritic metatexite	Lower	Undated rims	60.3550	4.9250
OC-08	404.8	5.2	1001	6	Granitic metatexite	Lower	High U	60.3933	5.0175
OC-09	401	14	1230	8	Migmatitic paragneiss	Lower	Rec. Pb loss	60.3338	5.0062

*Sorted by geological domain.

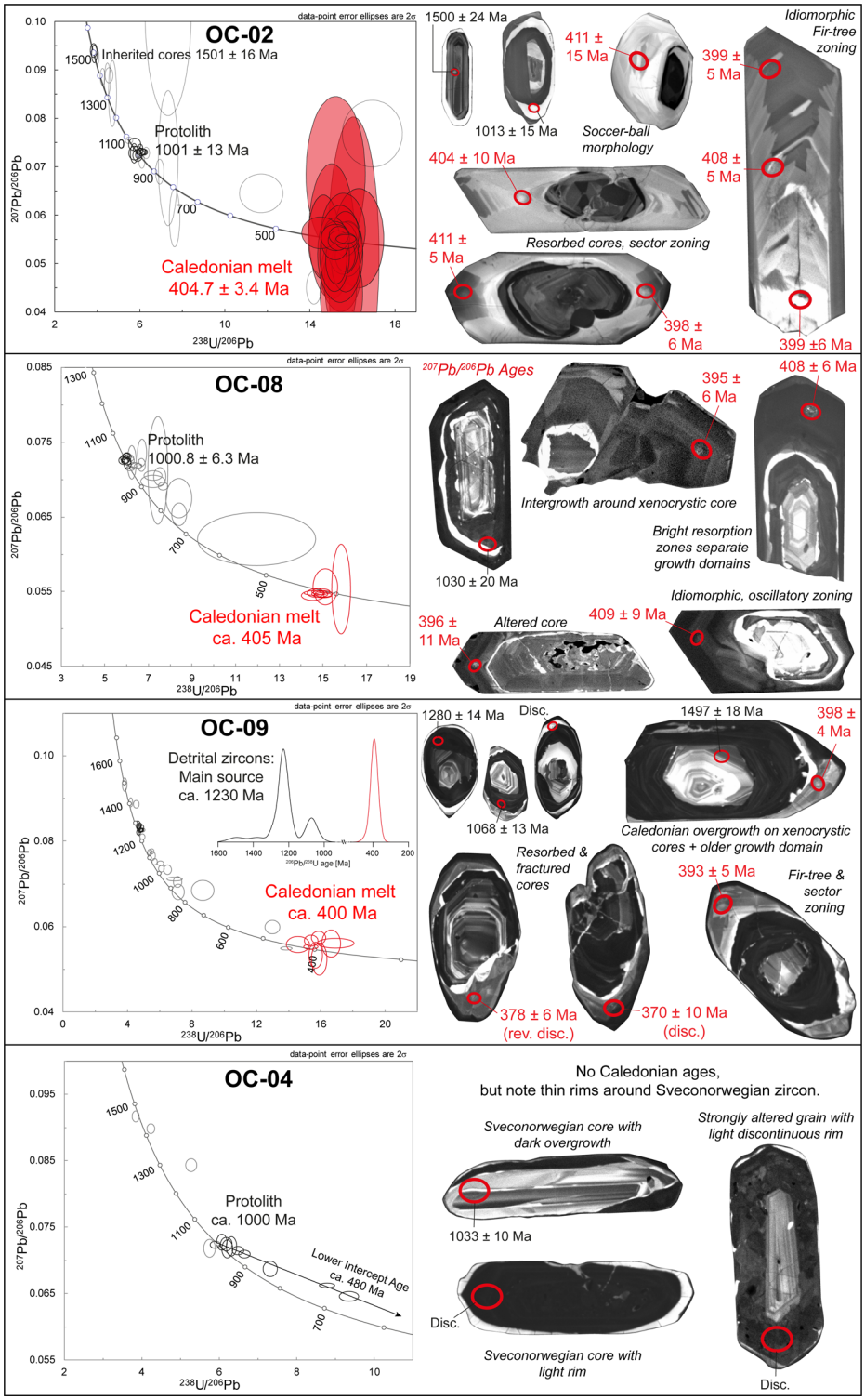

Fig. 5. Secondary ion mass spectrometry U–Pb zircon results shown in Tera–Wasserburg concordia diagrams (common Pb-corrected ratios) and annotated cathodoluminescence images of representative zircons. The size of the analysed spots marked by red ellipses corresponds to *c.* 10 μm diameter. The annotated ages are $^{206}Pb/^{238}U$ ages except for sample OC-08 ($^{207}Pb/^{206}Pb$ ages).

melanosomes (Supplementary Material ES-4). Locally, they grade into diffuse schlieren and connect to metre-wide granitic veins. The migmatitic fabrics are subvertical and were affected by pervasive ductile shearing of a weak intensity. The sampled leucosomes contain large (200–400 μm), brown to opaque idiomorphic zircons. They consist of resorbed xenocrystic cores, which are surrounded by oscillatory zoning or domains with simple zoning (Fig. 5). Separated through a resorption zone, some grains are surrounded by a second oscillatory/sector-zoned growth domain.

All of the 36 analysed spots have very high U (2000–6000 ppm) and one outlier has as much as 17 000 ppm U. Compared with the nearby sample OC-02, this implies a remarkable variation in U concentration across five orders of magnitude. No xenocrystic core was analysed. The first growth domain has moderate Th/U ratios (0.05–0.2) and gives a concordia age of 1001 ± 6 Ma (MSWD 1.9) for ten concordant analyses. By contrast, the second growth domain has significantly lower Th/U ratios (≤0.01) and gives nine $^{206}Pb/^{238}U$ ages ranging from 429 to 395 Ma. Seven of these analyses are slightly reversely discordant, whereas all have identical $^{207}Pb/^{206}Pb$ ratios (Fig. 5). Considering the high U of these analyses, this suggests that the resulting $^{206}Pb/^{238}U$ ages are relatively too old, which is a common phenomenon in SIMS analyses of high-U zircon (White and Ireland 2012). Therefore the $^{207}Pb/^{206}Pb$ weighted mean age of the nine youngest analyses of

404.8 ± 5.2 Ma (MSWD 1.05) seems more robust than their concordia age of 412.7 ± 2.8 Ma (MSWD 17).

OC-09

Collected near the Signalen hill, sample ØC-09 is a migmatitic paragneiss. The stromatic metatexite consists of ptygmatically folded centimetre-scale granitic leucosomes (Supplementary Material ES-4) with thin melanosomes and decimetre-scale granitic veins. The steep migmatitic fabrics have been overprinted and vertically shortened by solid-state shearing of moderate intensity. The sampled leucosomes contain intermediate size (150–300 μm) light brown to opaque euhedral zircons, commonly with rounded corners. The zircons have xenocrystic cores that are irregularly shaped and have been resorbed along their boundaries and internal fractures (Fig. 5). These cores are surrounded by two distinct growth domains. The inner domain has oscillatory zoning and is cathodoluminescence-dark, whereas the outer domain is cathodoluminescence-bright with broad zones, sector zoning and minor fir tree zoning.

The 42 analysed spots show a high variability in U (100–4500 ppm) and Th/U ratios (<0.001–0.8). Concordant ages occur in several groups at *c.* 1500, *c.* 1400, *c.* 1200 and *c.* 1100 Ma. The largest group at *c.* 1200 Ma, which relates to the inner (cathodoluminescence-dark) growth domain in the zircons, has U between 1000 and 2500 ppm and distinct Th/U ratios of *c.* 0.01. A cluster of ten concordant analyses gives a $^{206}Pb/^{238}U$ weighted mean age of 1230 ± 8 Ma (MSWD 1.7). By contrast, the outer cathodoluminescence-bright growth domain has U ≤500 ppm and bimodal Th/U ratios (*c.* 0.05 and *c.* 0.001). The corresponding $^{206}Pb/^{238}U$ ages range from 478 to 370 Ma and define a pronounced probability peak at 400 Ma (Fig. 5). No precise age can be calculated for this group as a result of the scatter of the data.

OC-04

Sample OC-04 was collected on the island of Algrøy in a heterogenous part of the migmatite complex, consisting of metatexites with granitic, mafic and intermediate compositions. Varying amounts of melt are found in folded stromatic leucosomes, shear bands and fractures (in amphibolites) and in larger granitic veins. The migmatitic fabrics are folded into recumbent folds and overprinted by shearing of moderate intensity. The sample was collected from a decimetre-scale granitic vein, which is connected to diffuse centimetre-scale schlieren in a layer of intermediate composition (Supplementary Material ES-4). It contains small (100–200 μm) light brown to transparent euhedral zircons with commonly rounded corners. The zircons show oscillatory or *c*-axis parallel zoning (Fig. 5), sometimes with xenocrystic cores. A number of grains show an overgrowth of thin irregular and often discontinuous rims on recrystallized and homogenized grains.

The 17 analysed spots are mostly discordant (Fig. 5) and show a large spread in Th/U ratios (0.05–1) and variable, but commonly high, U (500–7000 ppm). Three analyses of xenocrystic cores point towards a *c.* 1.5 Ga age. Ten analyses define a discordia with an upper intercept age of 1001 ± 17 Ma and a lower intercept at 483 ± 28 Ma (MSWD 0.93).

$^{40}Ar/^{39}Ar$ mica dating

Shear zones in the Gulen MCC are described in detail by Wiest *et al.* (2019) and the sampled shear zones in the Øygarden Complex are documented by Wiest *et al.* (2020*a*). The location of all samples is shown in Figure 4. In addition, we provide outcrop and thin section photographs of the samples in electronic Supplementary Material ES-4.

Gulen MCC

Detachment domain. G1 is a mylonitic gneiss from a sub-horizontal shear zone on the island Kversøyna. The quartz shows low-temperature/high-stress microstructures (regime 1–2 microstructures as defined by Hirth and Tullis 1992; Platt *et al.* 2015), whereas biotite and white mica form C-S structures indicating top-to-the-west kinematics. In the white mica sample, steps 2–17 provide a plateau age of 424.4 ± 6.9 Ma (G1m, Fig. 6). Biotite steps 2–19 define a plateau with a younger age at 418 ± 3.5 Ma (G1b, Fig. 6). Sample G2 is a garnet mica schist in a SSW-dipping shear zone in the Sløvågen area. Abundant white mica constitutes the foliation with dextral (top-to-the-west) fabrics. In the white mica sample, >95% of the released ^{39}Ar defines a plateau with an age of 410.4 ± 1.1 Ma (G2m, Fig. 6). Sample G4 is a mylonitic quartzite with top-to-the-west kinematics in a sub-horizontal shear zone at Rutleneset. Regime 1–2 quartz microstructures overprint high-temperature/low-stress microfabrics (regime 3 microstructures following Hirth and Tullis 1992; Platt *et al.* 2015) and white mica forms fishes parallel and oblique to the foliation. A plateau age of 402 ± 1.2 Ma (G4m, Fig. 6) can be calculated across the entire release spectrum of the analysed white mica.

Transitional domain. Sample G3 was collected from a sinistral vertical shear zone at the edge of a partially retrogressed eclogite lens on the island of Hille. Retrogression is marked by a front, which migrated from the rim to the core of the eclogite, and was induced by fluids (Wiest *et al.* 2019). The sampled granitic mylonite shows regime 2–3 microstructures and contains abundant large skeletal epidote/clinozoisite porphyroblasts, which locally pseudomorph garnet. White mica and biotite are abundant and appear chaotically intergrown. The white mica analyses yield a plateau over the entire degassing spectrum with an age of 404.9 ± 4.0 Ma (G3m, Fig. 6). For biotite steps 2–20, we calculate a younger plateau age at 400.4 ± 3.0 Ma (G3b). Sample G6 is a garnetiferous mylonitic gneiss from a sub-horizontal shear zone in Sleire. The sample shows symmetrical quartz ribbons with regime 2–3 microstructures and mica-rich shear bands with asymmetrical regime 1–2 fabrics indicating top-to-the-west kinematics. For white mica steps 4–12, we calculate a plateau age of 400.5 ± 3.0 Ma (G6m, Fig. 6). Biotite steps 10–23 yield a significantly older plateau age of 418.4 ± 2.1 Ma (G6b).

Core domain. Sample G5 was collected from a coarse-grained garnet mica schist layer, which occurs together with quartzites and gneisses in a subvertical shear zone on the island Sandøyna. Fabrics in the shear zone show sub-horizontal lineations, coaxial east–west stretching and lineation-parallel upright folds. In the schist, the latter are expressed as crenulations parallel to mineral stretching lineations. The quartz shows regime 2–3 microstructures, whereas biotite replaces garnet and is intergrown with large white mica fishes. The entire release spectrum of white mica defines a plateau with an age of 401.9 ± 2.3 Ma (G5m, Fig. 6). In the biotite sample, steps 5–23 yield a plateau age of 405.8 ± 2.2 Ma (G5b), which is within error of the white mica age estimate.

Transition to Southern WGR. Located in an NE–SW-striking coaxial shear zone on the mountain Svadfjellet, sample G7 represents upright folded (para)gneisses interlayered with granitic sheets. The symmetrical gneissic microfabric consists of coarse-grained white mica, feldspar and strain-free, recovered quartz. In the analysed white mica, steps 2–20 define a plateau for *c.* 90% of the released ^{39}Ar with an age of 393.4 ± 1.7 Ma (G7m, Fig. 6).

Nappes (Bergen Detachment)

Sample N1 was collected from a shallowly east-dipping top-to-the-east shear zone at the base of the Lindås Nappe on Herdla, structurally underlaying the Bergen Arc eclogites on Holsnøy (Austrheim 1987). The sample consists of a mylonitic amphibolite

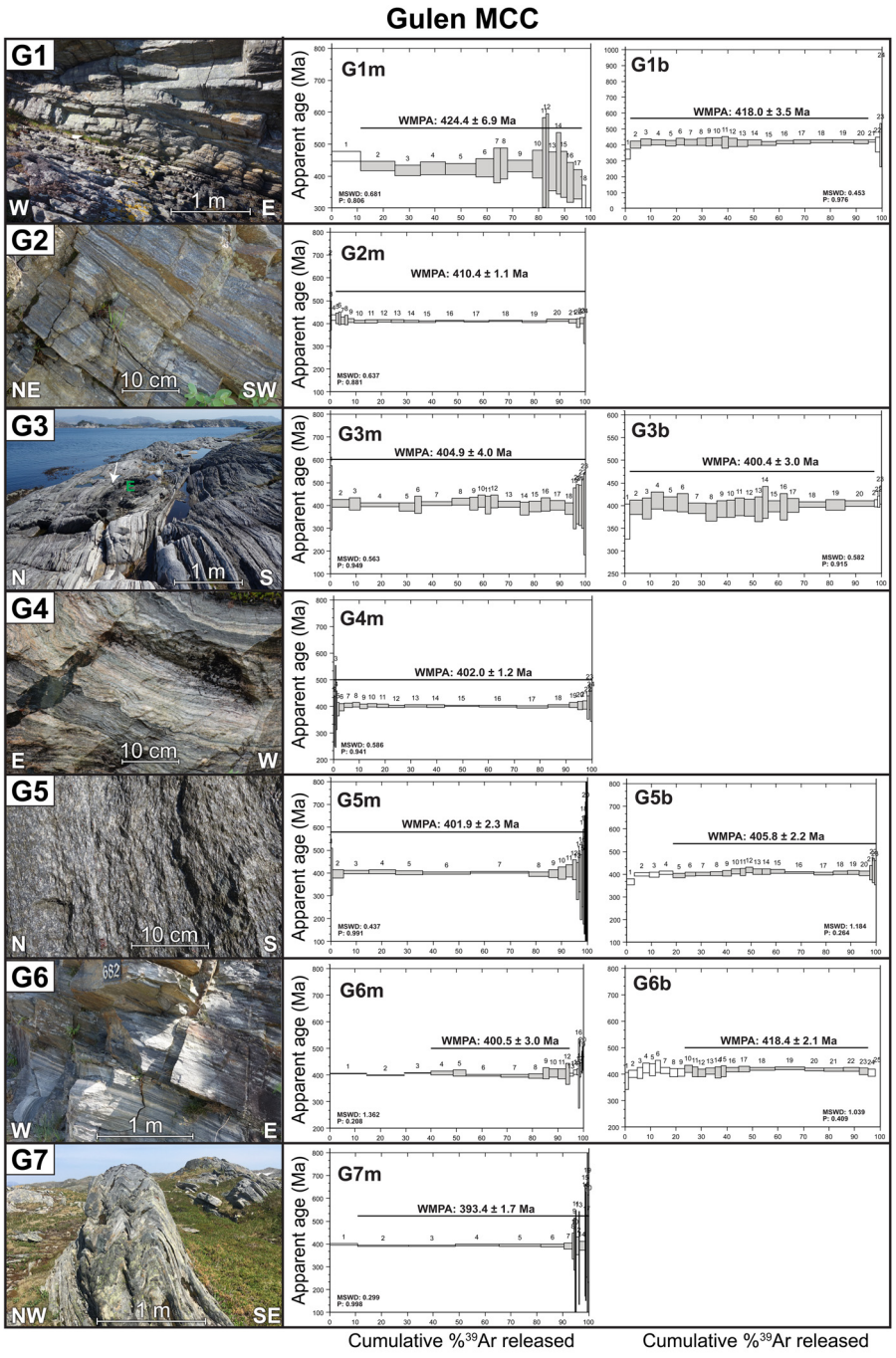

Fig. 6. Field photographs and degassing spectra of $^{40}Ar/^{39}Ar$ samples from the Gulen metamorphic core complex. Annotations for G3: E, eclogite; white arrow, sample location.

with retrograde biotite, epidote, minor white mica and chlorite. The mylonitic foliation is cut at a low angle by numerous asymmetrical shear fractures. White mica occurs as a retrograde overgrowth on feldspars and the degassing spectrum defines a plateau over *c.* 80% of the released ^{39}Ar with an age of 431.6 ± 2.0 Ma (N1m, Fig. 7). Coarse-grained biotite forms part of the mylonitic foliation and steps 4–20 (>80% of released ^{39}Ar) give a significantly older plateau age of 457.3 ± 2.1 Ma (N1b). Sample N2 was collected from a garnet mica schist in the city of Bergen, which belongs to the Minor Bergen Arc (Nordåsvatnet Complex, Hardangerfjord Nappe Complex; Fossen and Ragnhildstveit 2008). The mylonitic schist contains shear fractures and quartz veins and shows asymmetrical regime 1–2 fabrics indicating top-to-the-NE kinematics. Relict regime 3 fabrics are found in isolated quartz ribbons. For white mica analyses, a plateau age can be calculated over the entire degassing spectrum with an age of 408.4 ± 2.5 Ma (N2m, Fig. 7).

Øygarden Complex

Bounding shear zones/faults. Sample O1 is taken from the dextral Austevoll shear zone, which is part of the Sunnhordland Detachment (Norton 1987) and consists of a mylonitic granitic gneiss separated by a brittle fault zone from the weakly deformed Sunnhordland Batholith. Although the gneisses are considered part of the Øygarden Complex (Ragnhildstveit and Helliksen 1997), the Sunnhordland Batholith belongs to the upper part of the orogenic wedge (Andersen and Jansen 1987). The mylonite has an amphibolite facies foliation defined by biotite and regime 2–3 microstructures. It contains abundant allanite with epidote coronas and titanite, whereas minor white mica appears to have grown at the expense of feldspar. Fluid ingress along fractures is witnessed by abundant quartz veins and led to the minor chloritization of biotite. Although the content of white mica was too small to be dated, biotite steps 2–20 (>90% of released ^{39}Ar) give a plateau age of 410.3 ± 3.2 Ma (O1b, Fig. 7).

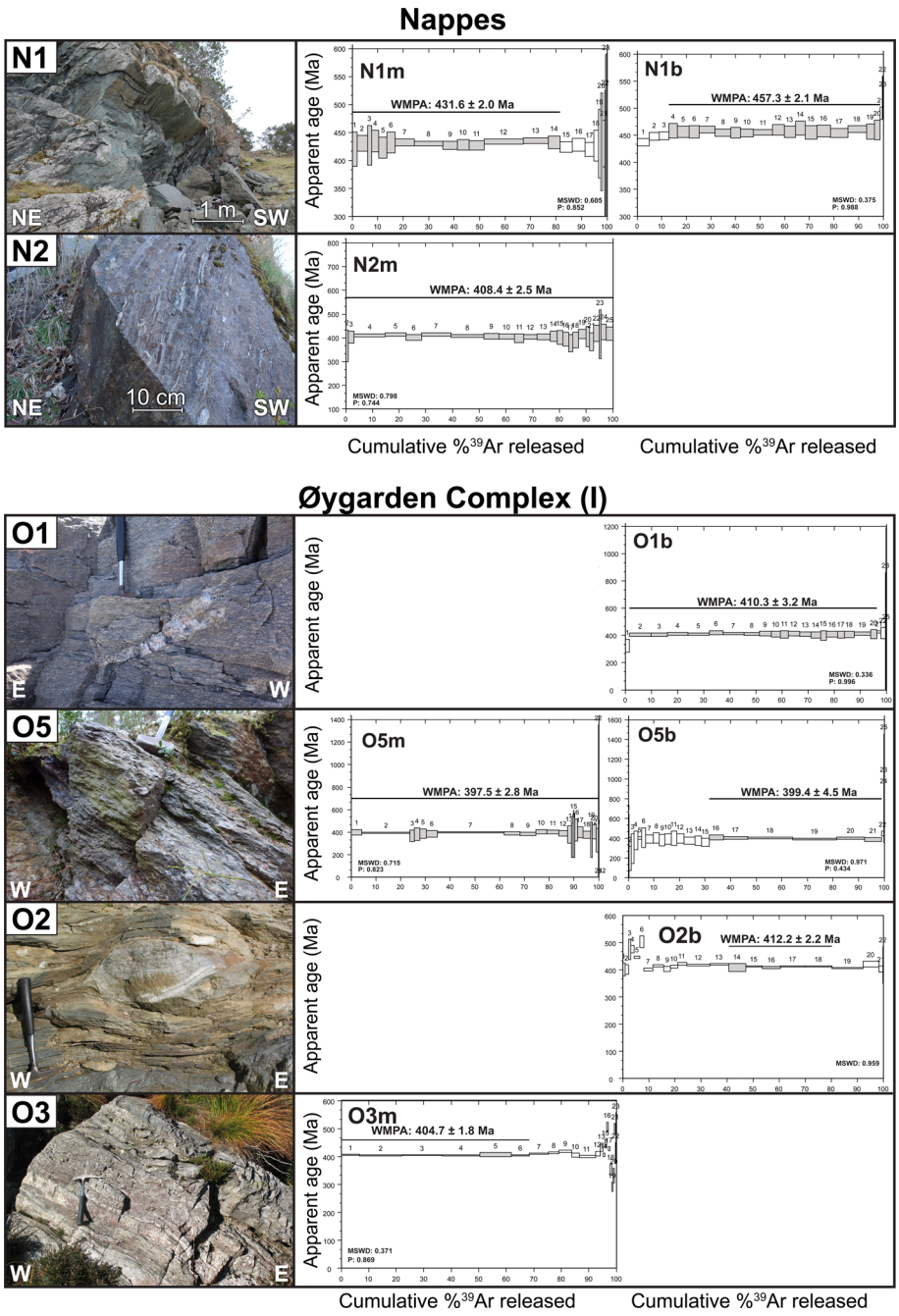

Fig. 7. Field photographs and degassing spectra of $^{40}Ar/^{39}Ar$ samples from the nappes and the Øygarden Complex (part 1).

Sample O5 is a garnet mica schist from the Hanevik shear zone, which represents the eastern boundary of the Øygarden Complex. The schist resembles similar lithologies in the overlying Minor Bergen Arc (e.g. sample N2), but is interlayered with amphibolites and gneisses and is therefore considered to be part of the Øygarden Complex (Fossen and Ragnhildstveit 2008). Quartz ribbons with regime 2–3 microstructures and shear bands with regime 1–2 fabrics define S-C structures that indicate clear top-to-the-east kinematics. White mica contains fine-grained opaque inclusions (possibly graphite) and is intergrown with biotite in large clusters. For white mica, a plateau age of 397.5 ± 2.8 Ma (O5m, Fig. 7) can be calculated across the entire spectrum. In biotite, the first 15 steps are heterogeneous, but steps 16–21 (>60% of the released ^{39}Ar) yield a plateau age of 399.4 ± 4.5 Ma (O5b), which is within error of the white mica age.

Upper unit. Sample O2 is a chlorite–biotite phyllonite from the Loddefjord shear zone, which has been described in detail by Wiest *et al.* (2018). Retrograde hydration of an amphibolite led to successive replacement of amphiboles by biotite and chlorite. The sample contains the least chloritized biotite of the zone, but fine intergrowths of chlorite could not be entirely avoided. Biotite gives a plateau at 412.2 ± 2.2 Ma (O2b, Fig. 7), but some of the first steps show anomalously old ages (up to 500 Ma, probably due to ^{39}Ar recoil). Collected from a nearby exposure of the Loddefjord shear zone, sample O3 is a muscovite–epidote–quartz phyllonite, which formed through the hydration of a feldspar-rich pegmatite (Wiest *et al.* 2018). White mica defines a plateau at 404.7 ± 1.8 Ma for *c.* 70% of the released ^{39}Ar (O3m, Fig. 7).

Sample O4 is a granitic S-C mylonite taken from the Klokkarvik shear zone in the SE corner of the complex. The sample is similar to O1, but with pervasive regime 1–2 microstructures overprinted on regime 3 fabrics. Fluids invaded the rock along fractures and the resulting quartz veins were mylonitized, showing ductile–brittle–ductile deformation cycles. White mica formed through the hydration of feldspars, whereas biotite was weakly chloritized. For white mica, steps 3–17 (*c.* 80% of released ^{39}Ar) give a plateau

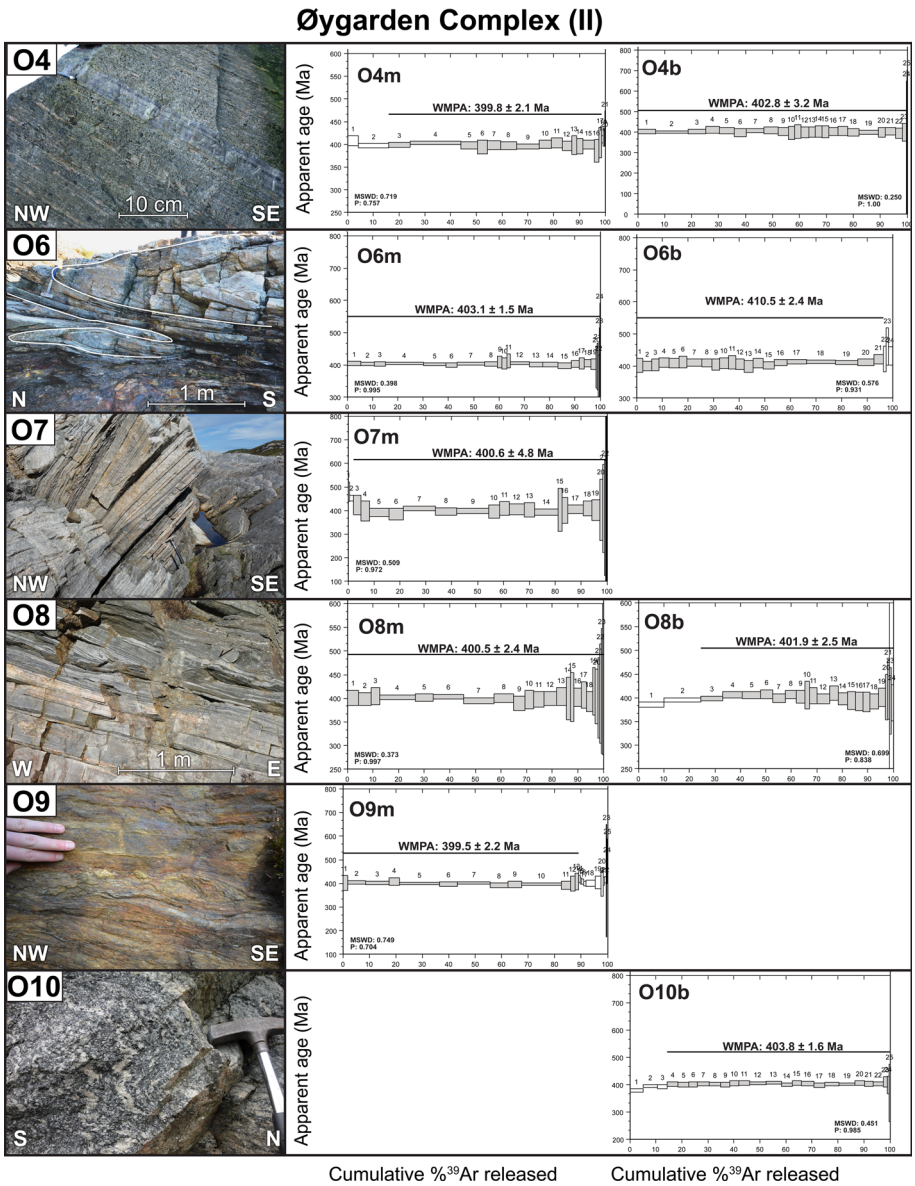

Fig. 8. Field photographs and degassing spectra of $^{40}Ar/^{39}Ar$ samples from the Øygarden Complex (part 2). White line in O6 traces isoclinal lineation-parallel folds. O9 photograph by Eric Salomon.

age of 399.8 ± 2.1 Ma (O4m, Fig. 8), whereas the entire degassing spectrum of biotite defines a plateau with an age of 402.8 ± 3.2 Ma (O5b).

Middle unit. Sample O6 is a mylonitic quartzite contained within a sillimanite–garnet–staurolite mica schist and forms a metre-scale sheath fold in the Alvheim shear zone. It mostly shows a regime 2–3 quartz microstructure with a CPO oblique to the main foliation, which is defined by large white mica crystals and quartz SPO. Biotite occurs as small grains in garnet strain shadows and is finely dispersed in interstitial positions. White mica gives a plateau over the entire spectrum with an age of 403.1 ± 1.5 Ma (O6m, Fig. 8). Biotite yields a significantly older plateau age of 410.5 ± 2.4 Ma (O6b) for >95% of the released ^{39}Ar.

Located on the northern flank of the Fedje dome, sample O7 is the northernmost sample from the Øygarden Complex. It was taken from the NW-dipping Kvalvika shear zone, which consists of interlayered schists, quartzites and mylonitic gneisses. The sampled garnet mica schist shows regime 3 microstructures overprinted by regime 1–2 fabrics and abundant ductile-to-brittle micro-shears. White mica degassing steps 3–25 (>95% of released ^{39}Ar) give a plateau age of 400.6 ± 4.8 Ma (O7m, Fig. 8).

Sample O8 of the Forland shear zone was collected just 2.5 km from sample O4. This is another mylonitic granitic gneiss with phyllonitic fabrics related to retrograde hydration. In contrast to sample O4, however, sample O8 shows top-to-the-west fabrics with pervasive regime 2–3 microstructures and only localized regime 1–2 fabrics in micro-shears. The latter formed along fractures, where fluids invaded the rock and white mica was growing. White mica yields a plateau age of 400.5 ± 2.4 Ma (O8m, Fig. 8) for the entire release spectrum, whereas biotite steps 3–24 (>70% of released ^{39}Ar) give a plateau age of 401.9 ± 2.5 Ma (O8b). Sample O9 is a garnet mica schist layer in the sub-horizontal, ductile-to-brittle Blom shear zone in the northern half of the complex. The schist contains mylonitized quartz veins with regime 2–3 microstructures and shear bands with a fine-grained phase mix and regime 1 microstructures. White mica occurs in large sigmoidal clusters, intergrown with brown biotite, and defines S-C structures. In this white mica sample, steps 1–13 (*c.* 90% of released ^{39}Ar) yield a plateau age of 399.5 ± 2.2 Ma (O9m, Fig. 8).

Lower unit. Sample O10 consists of the biotite melanosome surrounding the leucosome sampled for U–Pb zircon sample OC-02. The melanosome preserves a magmatic texture consisting of coarse-grained biotite, hornblende and minor feldspar and quartz. In the biotite degassing spectrum, steps 4–25 (85% of released ^{39}Ar) define a plateau with an age of 403.8 ± 1.6 Ma (O10b, Fig. 8), whereas the first three steps show slightly younger apparent ages.

Within uncertainties, the biotite plateau age of the melanosome is identical to the U–Pb zircon age of the leucosome (404.7 ± 3.4 Ma).

Discussion

Migmatization in the Øygarden Complex

The zircon population in the metatexite sample OC-02 gives clear textural evidence for zircon new-growth and overgrowths from a melt phase (Corfu *et al.* 2003), which crystallized at 404.7 ± 3.4 Ma. Based on the zircon characteristics and age relationships, the protolith of the migmatite is interpreted as a Sveconorwegian (1001 ± 13 Ma) migmatite or anatectic granite with inherited zircon cores as old as *c.* 1501 Ma, which confirms the Telemarkian affinity of the Øygarden Complex (Bingen and Solli 2009; Wiest *et al.* 2018). Discordant analyses apparently represent mixed core–rim analyses. The similar ages of the neighbouring sample OC-08 can equally be assigned to protolith crystallization at *c.* 1001 Ma and Caledonian melt crystallization at *c.* 405 Ma. However, sample OC-08 provides no precise age as a result of the relatively older $^{206}Pb/^{238}U$ ages compared with the $^{207}Pb/^{206}Pb$ ages, which is related to well-known issues in SIMS analyses of very high-U zircon (White and Ireland 2012). The migmatitic paragneiss OC-09 contains detrital zircons with a main population of early Sveconorwegian zircons (1230 ± 8 Ma). Similar to the previous samples, analyses of the outermost zircon growth domain constrain melt crystallization to *c.* 400 Ma, but the scatter of the ages inhibits the calculation of a precise age.

The timing of migmatization is less clear in sample OC-04 due to the lack of Caledonian ages. The most concordant ages of *c.* 1.0 Ga correspond to igneous zircon textures and chemistries. All the discordant analyses come from metamict zircon domains without textures indicative of partial melting and show a correlation between high U and low ages. Therefore the lower intercept age at 483 ± 28 Ma (which is not associated with concordant ages) is unlikely to correspond with the timing of partial melting. However, this age is well explained as the low-temperature resetting of high-U metamict zircon, as observed in (non-migmatitic) Sveconorwegian granites in the eastern Øygarden Complex (Wiest *et al.* 2018). Similar lower intercept ages can even be found in granites in the Sveconorwegian province of southern Norway (Coint *et al.* 2015), far away from the realm of Caledonian thick-skinned deformation. Hence the 1001 ± 17 Ma upper intercept age most likely represents the protolith age of sample OC-04, whereas Caledonian partial melting formed thin discontinuous zircon rims, but left no dateable evidence. In polymetamorphic terranes, it is not uncommon that samples with textural evidence for partial melting contain no dateable zircon (Gordon *et al.* 2013) and, even in diatexites, large parts of the zircon population can remain unaffected by anatexis (Keay *et al.* 2001).

In summary, three of the four U–Pb zircon migmatite samples from the Øygarden Complex contain Caledonian zircon and the concordia age from sample OC-02 robustly constrains melt crystallization at 404.7 ± 3.4 Ma. This age corresponds to the probability peak of the previously published U–Pb zircon ages of melts (*c.* 404 Ma) in the Central and Northern WGR (Gordon *et al.* 2013, 2016; Kylander-Clark and Hacker 2014). Located *c.* 200 km south from where Devonian melt has been previously dated, however, our new results largely expand the spatial extent of melting in the Caledonian infrastructure (Fig. 1). The difference between the Gulen dome (melt absent) and the Øygarden Complex (melt present), by contrast, highlights the highly variable rheological state of the ductile infrastructure during collapse. In many parts of the WGR, however, the presence or absence of Devonian melting remains poorly constrained. For example, Andersen *et al.* (1994) presented textural arguments for syn-deformational decompression melting in the dome north of the Gulen MCC, but geochronological evidence is lacking. Because the occurrence of even small amounts of melt has large implications for crustal rheology and orogen dynamics (Rosenberg and Handy 2005; Vanderhaeghe 2012), this clearly highlights the need for further studies in the Southern WGR.

$^{40}Ar/^{39}Ar$ dating: ductile flow in the Øygarden Complex and Gulen MCC

Most of the acquired $^{40}Ar/^{39}Ar$ mica dates fall in a narrow range between 410 and 398 Ma (Fig. 9), although there are some older outliers. The dataset shows no systematic variation between the Gulen MCC and the Øygarden Complex and, in the latter area, no difference between samples with top-to-the-west and top-to-the-east fabrics (Table 1). For shear zones where two micas have been analysed, the biotite and white mica ages are commonly identical within uncertainty, but in some cases the biotite ages are significantly older (G6, N1 and O2b v. O3m and O6). This is a commonly observed phenomenon in polymetamorphic areas (Stübner *et al.* 2017) and, in the case of our samples, there are several possible explanations. (1) Biotite usually forms part of the amphibolite facies gneissic foliation, whereas white mica occurs in several samples (e.g. N1, O3 and O6) as a retrograde product resulting from the hydration of feldspars. (2) Most samples show evidence of significant hydration by fluids. These fluids may have carried high concentrations of ^{40}Ar, which can be incorporated and lead to older biotite ages (McDonald *et al.* 2016). (3) Biotite is sometimes chloritized (e.g. samples N1b, O1b and especially O2b), which could cause anomalous older ages (Di Vincenzo *et al.* 2003). (4) Furthermore, a high number of dislocations in trioctahedral micas can increase Ar retentivity and cause older apparent ages (Camacho *et al.* 2012). Although biotite appears, unsurprisingly, to be the less reliable chronometer, we still report the analysed biotite dates for the sake of completeness, but they do not alter our geological interpretations, which are based on the white mica. We subdivide our dataset into four groups (Fig. 9), which can also be recognized in the results of previous studies in this area (Chauvet and Dallmeyer 1992; Boundy *et al.* 1996; Fossen and Dunlap 1998, 2006).

Group 1: pre-Devonian ages (>415 Ma)

The first group comprises five dates ranging from *c.* 460 Ma to *c.* 418 Ma (Fig. 9). Sample N1 from the base of the Lindås Nappe gives the oldest acquired ages for biotite (*c.* 460 Ma) and white mica (430 Ma). These ages precisely reproduce previous ages from the Lindås Nappe (Fossen and Dunlap 1998; Schneider *et al.* 2008), but contradict the ages of eclogite formation and partial melting in the same unit (Kuhn *et al.* 2002; Bingen *et al.* 2004). The homogeneous, but geologically meaningless, dates from the Lindås Nappe might relate to the commonly dry protoliths in this nappe (Austrheim 1987; Schneider *et al.* 2008). At the western apex of the Gulen MCC, sample G1 gave ages for both micas that were considerably older than other samples in the area. However, large variations in the degassing spectrum of G1m suggest that inhomogeneities or excess Ar could be responsible for the old age. Alternatively, this sample might represent part of the upper plate Caledonian allochthons that were folded into the detachment zone. In sample G6 (Fig. 6), the biotite age (G6b, 418.4 ± 2.1 Ma) is 18 myr older than the white mica (G6m, 400.5 ± 3.0 Ma), but there is no obvious explanation for this difference.

Group 2: detachment shearing and MCC exhumation (410–398 Ma)

Five dates around 410 Ma (Fig. 9) correspond to previously published ages from the nappes that are mostly associated with top-

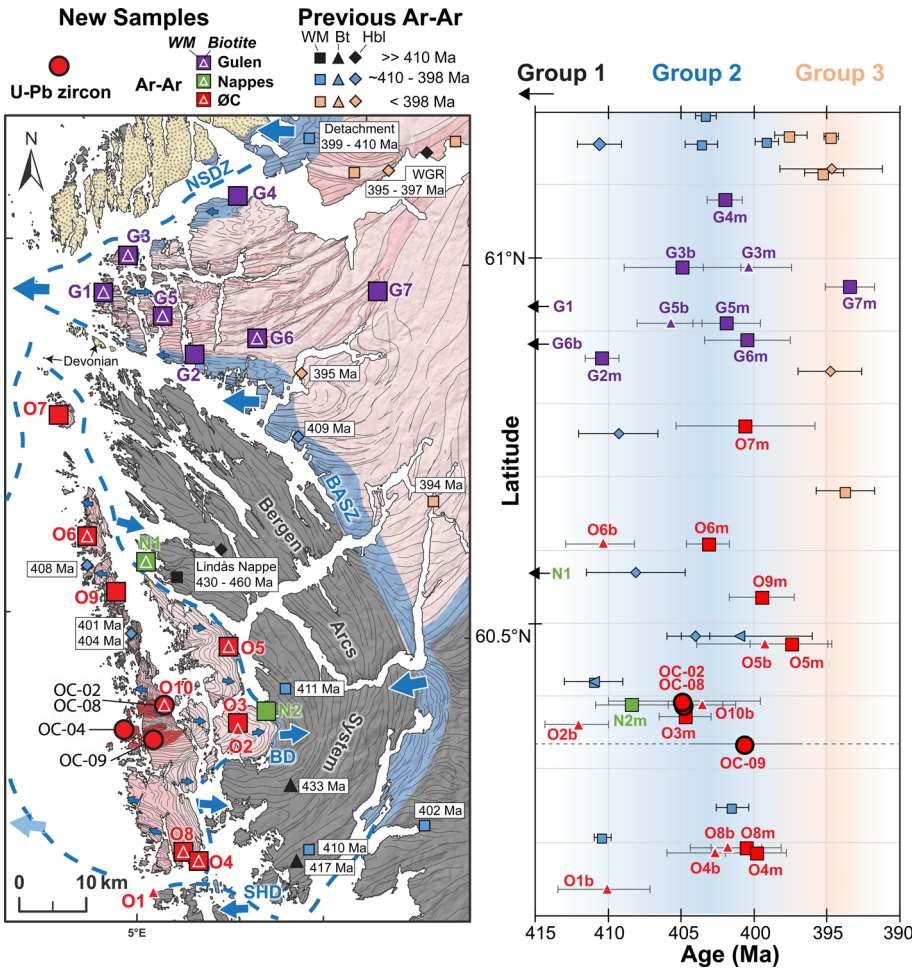

Fig. 9. New and previous geochronology plotted against latitude corresponding to the sample map, which shows the samples in relation to detachments, shear sense and deformation domains (see Fig. 4 for legend).

to-the-east fabrics and therefore interpreted to date the late stages of Scandian thrusting (Fossen and Dallmeyer 1998; Fossen and Dunlap 1998, 2006). In the case of our samples, white mica dated to this age comprises top-to-the-west (G2m) and top-to-the-east fabrics (N2m). A simple distinction between thrusting- and collapse-related fabrics is not possible because extension was bivergent in this part of the orogen (Wiest *et al.* 2020*a*). The oldest biotite ages in this group are commonly associated with chlorite impurities (O2b and O1b), which might have caused older apparent ages and makes these ages less reliable. In general, however, all of the ages of *c.* 410 Ma come from samples collected close to or within the detachment zones (Fig. 9), which could indicate that the onset of detachment shearing occurred at *c.* 410 Ma.

Most white mica $^{40}Ar/^{39}Ar$ ages from both MCCs fall into a narrow time period between 405 and 398 Ma, conforming to most ages from previous studies and overlapping with the SIMS U–Pb zircon age of melt crystallization in the Øygarden Complex (Fig. 9). In many of these samples, the biotite analyses show well-defined plateaus and the ages of both micas overlap within error. The biotite sample O10b (403.8 ± 1.6 Ma) consists of the melanosome around the leucosome U–Pb zircon sample OC-02 (404.7 ± 3.4 Ma). The identical age suggests that the migmatite core must have cooled rapidly after melt crystallization. The narrow range of $^{40}Ar/^{39}Ar$ ages in both MCCs implies that the eclogite-bearing crust in the Gulen MCC and the partially molten crust in the Øygarden Complex were rapidly exhumed and cooled to ductile–brittle transition conditions. This conforms well with the onset of brittle faulting dated at *c.* 396 Ma in the Øygarden Complex (Larsen *et al.* 2003) and previous age interpretations (Boundy *et al.* 1996; Fossen and Dunlap 1998).

Group 3: unroofing of the Southern WGR (c. 396–393 Ma)

Sample G7m is located at the gradual transition from the Gulen MCC to the Southern WGR and shows the only younger age at 393.4 ± 1.7 Ma. Similar ages can be recognized in previously published data from areas inside the Southern WGR that are located away from the detachment zones (Fig. 9). A possible explanation for this pattern is that the exhumation/cooling of the basement in the Southern WGR took longer than in the MCCs, where the combination of detachment faulting and ductile flow rapidly exhumed the deep crust. However, more data are necessary to test the significance of this difference.

Geochronological segmentation of the WGR

Our new data add substantially to the geochronological record of the Southern WGR and allow for a more robust first-order comparison between distinct segments of the WGR (Fig. 10). Our $^{40}Ar/^{39}Ar$ data confirm that there is no age younger than *c.* 393 Ma in the Southern WGR. The youngest ages in the 50-km-scale domes in the immediate footwall of the Nordfjord–Sogn Detachment are *c.* 398 Ma. In the Central WGR, this time corresponds to the peak of melt crystallization ages (410–394 Ma) (Kylander-Clark and Hacker 2014), while most $^{40}Ar/^{39}Ar$ ages are significantly younger (390–375 Ma) and the U–Pb titanite, monazite and rutile ages overlap with both (*c.* 410–380 Ma). The overlap suggests that distinct geochronometers variably relate to different processes in the ductile crust – such as metamorphic reactions, recrystallization, fluids or diffusional resetting – rather than simple cooling below a closure temperature (Warren *et al.* 2012; McDonald *et al.* 2016).

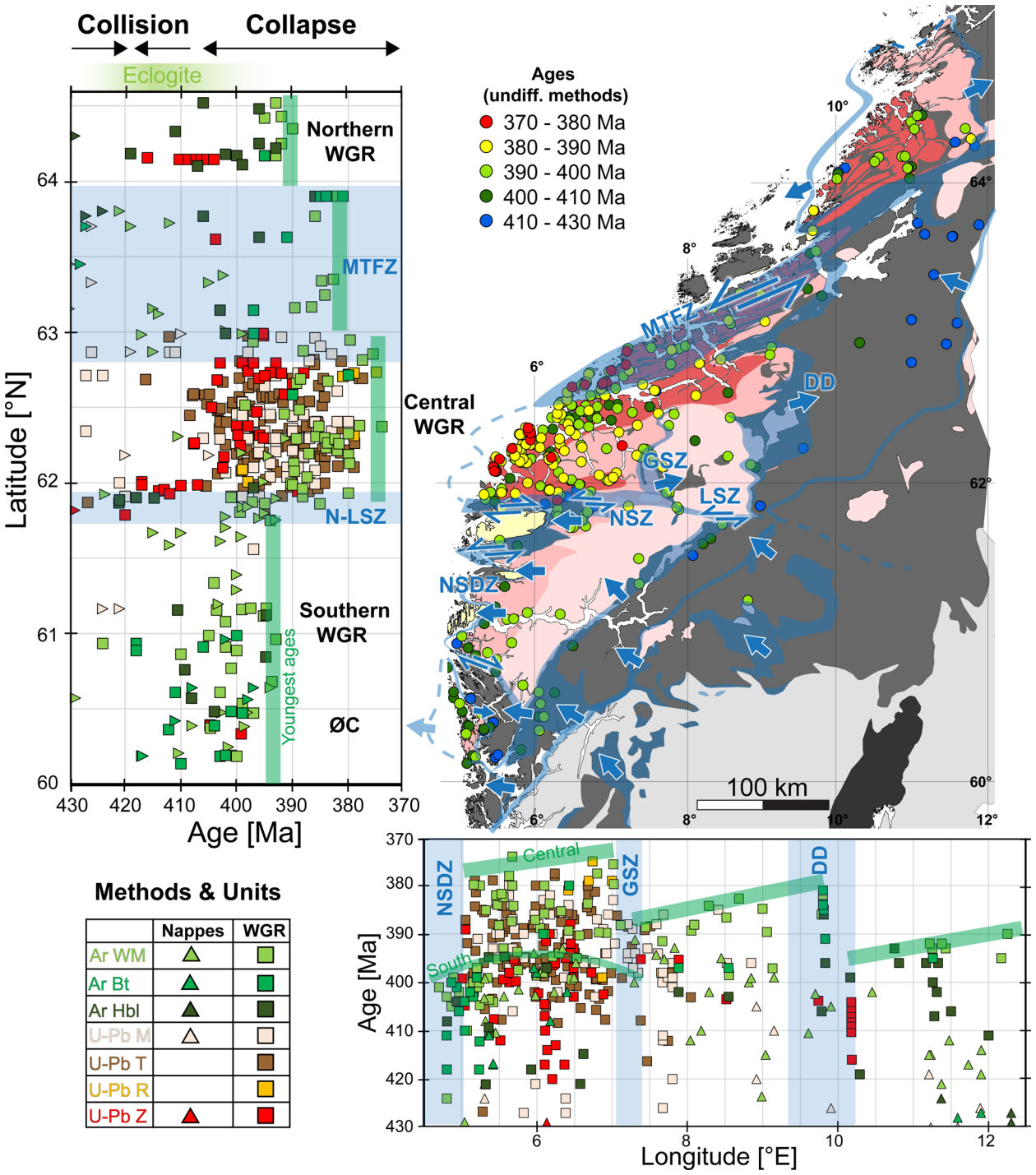

Fig. 10. Compiled geochronology of the Western Gneiss Region and overlying allochthons plotted on a map and as age v. latitude–longitude plots. The map distinguishes only five age groups, whereas the latitude–longitude plots differentiate dating techniques (colours) and units (Western Gneiss Region v. nappes). The limits of the youngest ages in each segment (marked by green bars) show major breaks across Devonian shear zones (see Fig. 2 for abbreviations). $^{40}Ar/^{39}Ar$ dating: Bt, biotite; Hbl, hornblende; WM, white mica. U–Pb dating: M, monazite; R, rutile; T, titanite; Z, zircon. WGR, Western Gneiss Region; see Figure 2 for map legend and further abbreviations.

Although we do not discuss geochronometer behaviour in detail, we want to point out significant variations in the range of the youngest ages in different domains.

As described here, various chronometers show a first-order trend from old ages in the SE to young ages in the NW, conforming to the subduction-related, first-order gradients of the peak metamorphic conditions and deformation intensity (Hacker *et al.* 2010; Spencer *et al.* 2013; Walsh *et al.* 2013). Second-order variations in the geographical distribution of ages, however, are not as gradual as expected for the postulated exhumation of a coherent slab (cf. Hacker *et al.* 2010; Kylander-Clark and Hacker 2014). All ages in the hanging wall of the Dovrefjell Detachment are >400 Ma, whereas ages <390 Ma are only found in the footwall of the east-directed Geiranger Shear Zone and its diffuse northern continuation (Fig. 10). The most significant break in the youngest ages (*c.* 20 myr, Fig. 10) occurs across the sinistral Nordfjord Shear Zone (Labrousse *et al.* 2004). Based on the assumption that the different radiometric ages record processes in the ductile regime, the youngest ages in each area may be simplistically interpreted as the closure of the ductile system. Hence the duration of ductile

behaviour was highly variable in different segments of the WGR (Fig. 11a). In the following, we compare these geochronological variations with contrasting structural regimes.

Structural segmentation of the WGR

Most of the Scandinavian Caledonides show four distinct deformation regimes from foreland to hinterland (Fig. 11a): regime I, foreland fold–thrust belt unaffected by extension; regime II, thin-skinned extension reactivating the basal décollement; regime III, planar detachments cross-cutting the basal décollement associated with low amplitude, extension-perpendicular footwall domes with weak internal deformation, partly preserving thrusting/imbrication structures; and regime IV, curved detachments exhuming strongly deformed (± partially molten) basement in extension-parallel domes (Eskola 1948; Krill 1985; Fossen and Rykkelid 1992; Milnes *et al.* 1997; Andersen 1998; Fossen 2000; Osmundsen *et al.* 2005; Fossen *et al.* 2014). Along the strike of the orogen, however, there are significant variations. For example, the gradual transition from regime I to IV occurs over *c.* 100 km in the Hardanger–Bergen area (Fig. 3, section E–E′), whereas it occurs over several hundred kilometres east of the Central WGR. Correspondingly, the sizes of the strongly deformed domains correlate to the inferred timing of ductile behaviour (Fig. 11a). In the Southern WGR, the strongly deformed basement was exhumed in relatively small MCCs with up to 50 km in

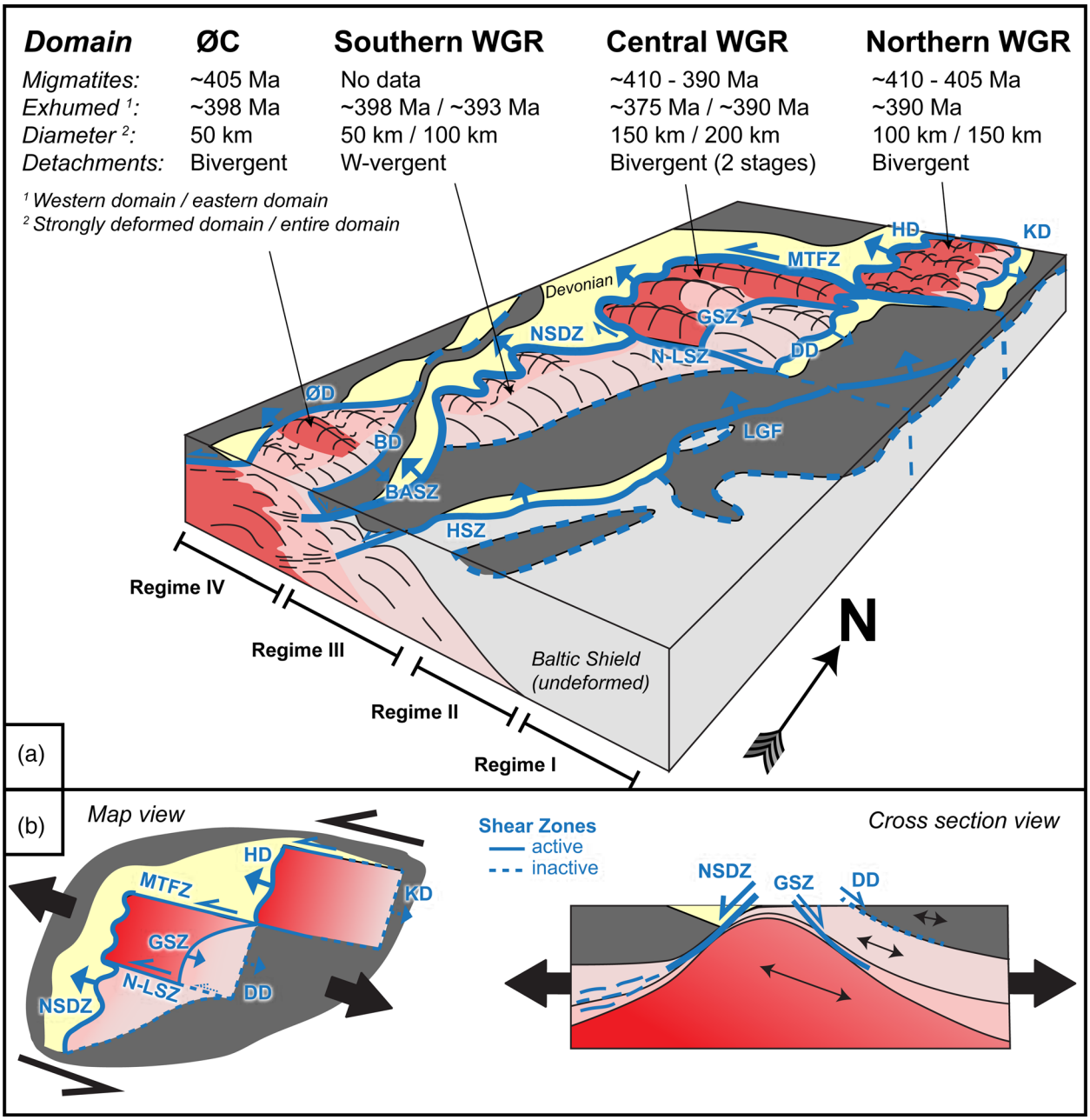

Fig. 11. (**a**) Schematic block diagram (perspective view from SE) illustrating along- and across-strike segmentation of the Western Gneiss Region. (**b**) Two-stage metamorphic core complex exhumation of the Central Western Gneiss Region. The cross-section illustrates schematically how the Dovrefjell Detachment was succeeded by the Geiranger Shear Zone as an antithetic detachment to the Nordfjord–Sogn Detachment Zone in response to non-uniform crustal stretching. The schematic map portrays the situation of the Central Western Gneiss Region in a releasing bend between sinistral transfer zones (the Møre–Trøndelag Fault Zone and the Nordfjord–Lom Shear Zone). DD, Dovrefjell Detachment; GSZ, Geiranger Shear Zone; MTFZ, Møre–Trøndelag Fault Zone; NLSZ, Nordfjord–Lom Shear Zone; NSDZ, Nordfjord–Sogn Detachment Zone; WGR, Western Gneiss Region. See Figure 2 for legend to colour scheme and further abbreviations.

diameter (e.g. the Gulen MCC and the Øygarden Complex) and the ages reflect short-lived ductile behaviour (*c.* 410–400 Ma). The strongly deformed domain of the Northern WGR measures *c.* 100 km across and the available ages suggest that ductile flow was largely completed at *c.* 390 Ma (except for younger ages within the Høybakken Detachment). The Central WGR exhibits the largest strongly deformed domain (120–200 km wide) and the longest duration of ductile behaviour (410–380 Ma).

The Devonian detachment system is asymmetrical and dominantly hinterland-directed (Fossen 2010). The highest metamorphic grades, finite strain and the youngest ages are correspondingly found in the immediate footwall of west-directed detachments. Except for the Southern WGR (Fig. 11a), antithetic foreland-directed detachments developed as secondary structures (Osmundsen *et al.* 2003) to accommodate large amounts of non-uniform crustal stretching (Fossen *et al.* 2014). Along the strike of the Nordfjord–Sogn Detachment, the amplitude and tightness of folds increases gradually from south to north, together with the depth of the exposed crustal section, but there is a marked structural break across Nordfjord (Fig. 3, section A–A′). In this area, isobars and isotherms (Hacker *et al.* 2010, their fig. 1) deviate from the straight NE–SW trend that might be expected for cylindrical northwestward subduction followed by south-eastward eduction. By contrast, they show differential fold patterns that increasingly align with the structural fold pattern towards higher pressures. The variably tight spacing of isobars indicates locally very steep pressure gradients (e.g. in the Nordfjord area), which imply the omission of significant crustal section or, in other words, that different levels of the orogenic crust were laterally juxtaposed.

The relationships in the Central WGR can be explained as two-stage MCC exhumation, possibly representing a highly asymmetrical analogue to the Menderes massif (Gessner *et al.* 2013). In the first stage (*c.* 405–390 Ma), the basement was dragged out from underneath the nappes forming the antithetic Dovrefjell Detachment. Continued crustal stretching (*c.* 390–375 Ma) formed the Geiranger Shear Zone as a successive antithetic detachment and progressively exhumed deeper crustal levels, including the partially molten and UHP domains (Fig. 11b). The kinematic role of the Møre–Trøndelag Fault Zone as a sinistral transfer zone has been established previously (Krabbendam and Dewey 1998; Braathen *et al.* 2000). We speculate that a similar role for the Nordfjord–Lom Shear Zone (Fig. 11b) can explain structural–metamorphic–chronological discontinuities across the southern boundary of the Central WGR. If future structural and geochronological evidence confirm this interpretation of the Nordfjord–Lom Shear Zone, then the Central WGR can be seen as a huge strike-slip MCC (Denèle *et al.* 2017) formed in a releasing bend between sinistral transfer zones (Fig. 11b).

Tectonic evolution of orogenic collapse

Based on the previous discussion, we present a refined model of the late- to post-orogenic Caledonian evolution in three stages (Fig. 12).

*Subduction to eduction (*c. *410–405 Ma)*

The broadly similar structure and timing of collision initiation along the length of the Scandinavian Caledonides (Corfu *et al.* 2014; Slagstad and Kirkland 2018) suggests a largely cylindrical orogen (Fig. 12a) comparable with the Himalayan system (Gee *et al.* 2010; Labrousse *et al.* 2010; Streule *et al.* 2010). During Scandian continental collision (>410 Ma), the rigidity of the Baltic Shield allowed coherent continental subduction and the prolonged burial of buoyant continental crust (Butler *et al.* 2015). This conforms with the limited number of ages from the WGR older than 410 Ma, compared with various nappes that were deeply buried, partially molten and variably exhumed in the subduction channel (Kuhn *et al.* 2002; Jolivet *et al.* 2005; Root and Corfu 2012). The allochthons, however, include distal parts of the Baltican margin (Jakob *et al.* 2019) and the folding of mantle rocks and nappes into the WGR further complicates the distinction of units (Labrousse *et al.* 2004, 2011; Young and Kylander-Clark 2015; Brueckner 2018; Walczak *et al.* 2019).

The number of U–Pb zircon ages of crystallized melts in the WGR increases significantly at *c.* 410–405 Ma, corresponding to the proposed switch from plate convergence to divergence (Fossen and Dunlap 1998). Our results from the Øygarden Complex show that partial melting also occurred at this stage in parts of the WGR that did not experience (U)HP metamorphism. This conforms with the argument of Kohn *et al.* (2015) that the lower plate underwent (isothermal) decompression from *c.* 410 Ma. The break-off of the oceanic lithosphere and the associated loss of slab pull (Duretz *et al.* 2012; Butler *et al.* 2015) provide a plausible cause for the near-instantaneous cylindrical eduction of the continental slab (Andersen *et al.* 1991), resulting in extensional reactivation of the basal décollement (Fossen 1992, 2000). The asthenosphere replacing the detached oceanic slab would have further increased the geothermal gradient of the collapsing orogen (Warren 2013).

*Root collapse, segmentation and MCC stage 1 (*c. *405–395 Ma)*

Thermal softening of the orogenic root (Fig. 12b) resulted in buoyancy- and isostasy-driven crustal flow overtaking slab eduction as the principal exhumation mechanism (Duretz *et al.* 2012). In the geochronological record, this stage corresponds to a large number of different mineral ages in the WGR between *c.* 405 and 395 Ma, which are widespread in the hinterland of the orogen. Oblique plate divergence (Krabbendam and Dewey 1998; Fossen 2010) was partitioned across the orogen as a result of the variable crustal rheology (recognized in different deformation regimes, Fig. 11a). Cylindrical deformation dominated cool and rigid cratons in the foreland (Fig. 12b), whereas transtension caused constrictional shearing of the ductile infrastructure in the hinterland (Fossen *et al.* 2013). At the transition, the paired Hardangerfjord–Moho shear zone developed as a zipper-like structure (Fossen *et al.* 2014). The rheological layering of the orogenic crust in the hinterland (soft infrastructure v. strong nappes; Fauconnier *et al.* 2014; Fossen *et al.* 2017) inevitably led to disruption of the orogenic wedge (Brueckner and Cuthbert 2013) and crustal-scale doming (Huet *et al.* 2011; Labrousse *et al.* 2016). Variations in the volumes of ductile material (Fig. 11a), however, caused segmentation of the infrastructure along the strike of the orogen (Fig. 12b). From *c.* 400 Ma, the first MCCs exhumed parts of the ductile infrastructure below the detachments and simultaneously formed collapse basins (Séguret *et al.* 1989). The ductile evolution of small MCCs, such as the Øygarden Complex and the Gulen MCC, was completed in this stage and minor subsequent crustal thinning occurred by brittle faulting (Larsen *et al.* 2003).

*MCC stage 2 (*c. *395–375 Ma)*

Large volumes of ductile material in the Central WGR caused a second stage of MCC exhumation during continued crustal stretching (Fig. 12c). This is documented by the succession of the Dovrefjell and Geiranger shear zones as antithetic detachments (Fig. 11b) and led to the exhumation of the deepest crustal levels (including the UHP domains), which are associated with the youngest ages (Fig. 10). At this stage, progressive transtension had rotated the divergence vector from orogen-perpendicular to near

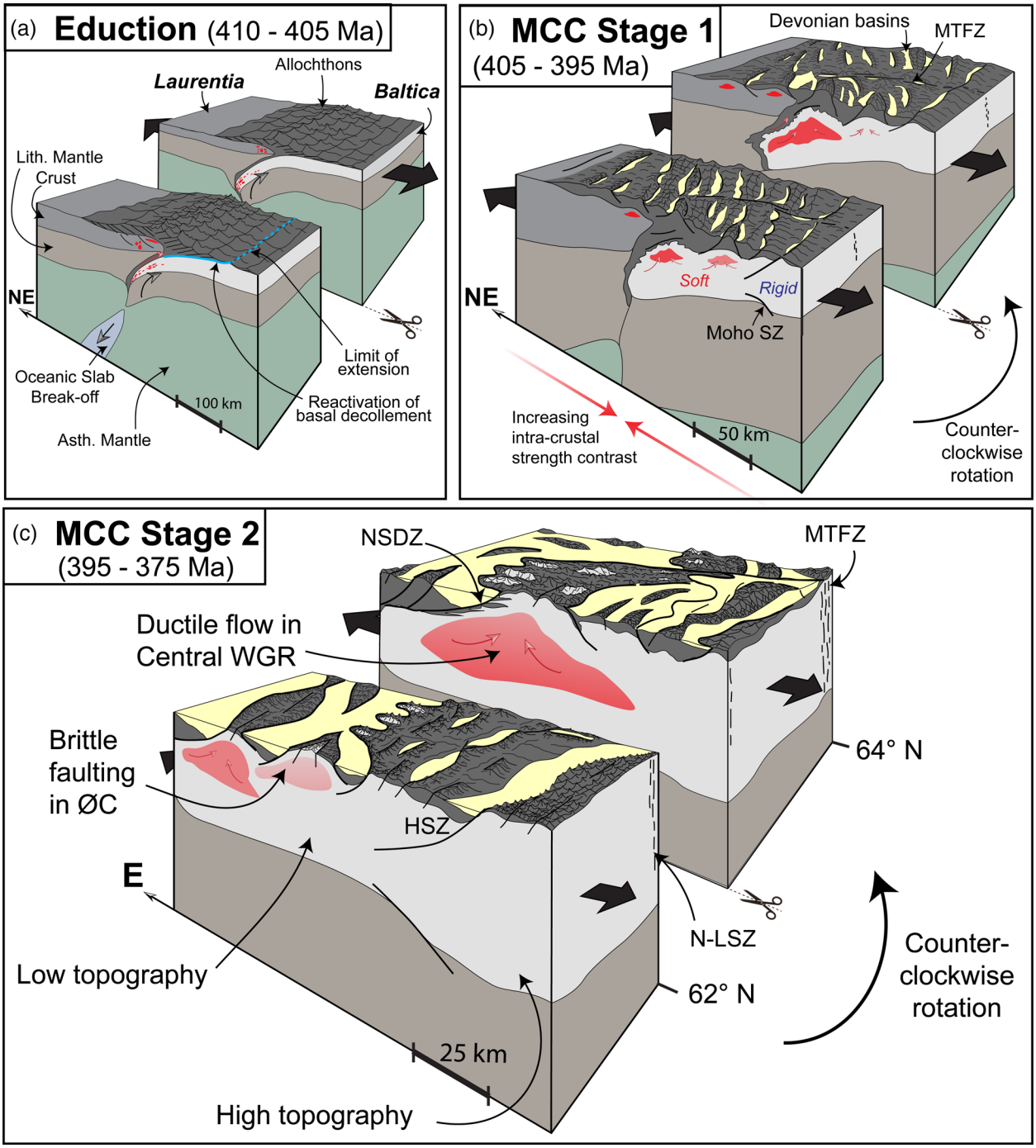

Fig. 12. Schematic block diagrams illustrating the evolution of orogenic collapse in three stages. Each block is cut open in the middle and presents a zoom-in from the previous stage; note change in scale and different orientation in part (c). Across-strike sections in part (a) and (b) are based on figure 3 from Duretz *et al.* (2012). Moho shear zone based on Fossen *et al.* (2014). HSZ - Hardangerfjord Shear Zone; MCC, metamorphic core complex; MTFZ, Møre–Trøndelag Fault Zone; N-LSZ, Nordfjord–Lom Shear Zone; NSDZ, Nordfjord–Sogn Detachment Zone; ØC, Øygarden Complex; SZ, shear zone; WGR, Western Gneiss Region.

orogen-parallel and ductile shearing was largely dominated by sinistral transfer zones. This explains why we find the highest metamorphic grades (Engvik *et al.* 2018) and youngest ages (Butler *et al.* 2018) in the vicinity of the Møre–Trøndelag Shear Zone and the progressive rotation of structural trends towards the shear zone (Osmundsen *et al.* 2006; Fossen *et al.* 2013). The youngest ages of *c.* 375 Ma indicate that collapse-related ductile deformation diminished in the Late Devonian. Parts of the former orogenic infrastructure were exhumed to the surface and were a source for extensive Devonian basins (Eide *et al.* 2005; Templeton 2015), which were buried to depths of up to 13 km (Svensen *et al.* 2001; Souche *et al.* 2012).

Implications

Continental transfer zones: dynamic instabilities or structural inheritance?

Our model invokes a crucial role of transfer zones between low-angle detachments. However, the strike-slip shear zones received comparably little attention and remain incompletely understood. We note that the location of the Lom Shear Zone at the border of the Central and Southern WGR corresponds to a break in the nappe architecture of the orogenic wedge, separating distinct nappe complexes. Jakob *et al.* (2019) interpret this as segmentation of the pre-Caledonian Baltican margin following an inherited

Sveconorwegian lineament. Seranne (1992) argued that the Møre–Trøndelag Fault Zone originated as a transpressional structure. The locations of the transfer zones, which facilitated segmentation during post-orogenic collapse, could therefore correspond to long-lived weak zones in the lithosphere that influenced different stages of the orogenic evolution.

By contrast, the continental transfer zones in Western Norway (Fig. 11b) resemble transform faults at mid-oceanic ridges. While oceanic transform faults can evolve in plane strain through the growth of ridge curvature related to dynamic instabilities (Gerya 2010), a similar evolution might be envisaged for continental extension with a high intra-crustal strength contrast between brittle and ductile layers (Le Pourhiet *et al.* 2012; Cao and Neubauer 2016; Labrousse *et al.* 2016). In the case of the Møre–Trøndelag Shear Zone, this would correspond to rigid ophiolitic rocks in the nappes overlying a soft (partially molten) WGR. This would also conform with the postulated formation of this shear zone through progressive localization from a wide belt of folded rocks (Osmundsen *et al.* 2006). In summary, the location of strike-slip shear zones in Western Norway seems best explained by inherited lithospheric weak zones, while their development was probably facilitated by dynamic instabilities during transtension.

Long-term lithospheric evolution

The syn-collisional architecture of the Caledonian orogen was largely preserved in the foreland fold–thrust belt, whereas the present structure of the WGR is largely the result of post-orogenic transtensional collapse. In the hinterland of the orogen, the combination of ductile flow, erosion and sedimentation provided an effective means of mass redistribution that removed the overthickened crust, and thereby the cause of the high topography, by the Middle to Late Devonian (Fig. 12c). Around the Gulen MCC, for example, the crustal thickness was no more than *c.* 40 km at this time (Wiest *et al.* 2019). Apparently, a larger crustal thickness was preserved towards the foreland, where collapse mechanisms were less effective because of lower rates of ductile flow (strong rheology; Fig. 12b) and erosion (initially lower and less steep topography; Fig. 12a). This is marked by a stepwise increase in crustal thickness across the paired Hardangerfjord–Moho shear zones (Fig. 12c; Fossen *et al.* 2014), which corresponds today to a significant step from low topography at the west coast to high topography on Hardangervidda. Hence collapse rapidly modified the wavelength and amplitude of the inherited Caledonian crustal anomaly, but the effects were spatially highly variable. This has important implications for later North Sea rifting (Christiansson *et al.* 2000; Fazlikhani *et al.* 2017; Wiest *et al.* 2020*b*), the formation of the Norwegian margin (Peron-Pinvidic and Osmundsen 2020) and the long-term topographic evolution (e.g. Gabrielsen *et al.* 2010; Pedersen *et al.* 2016).

Summary and conclusions

To refine models of Caledonian collapse, we compared the structures and geochronology of infrastructure windows in a >600 km wide section of the orogen and provide new ages from poorly dated windows. In the Øygarden Complex, three of four migmatite samples reveal Caledonian U–Pb zircon ages and sample OC-02 robustly constrains leucosome crystallization at 404.7 ± 3.4 Ma. This age corresponds to the main period of melt crystallization in the WGR, but significantly expands the spatial extent of documented Devonian melting. White micas from shear zones in and around the Øygarden Complex and Gulen MCC reveal $^{40}Ar/^{39}Ar$ flat incremental heating release spectra and plateau ages mostly between 410 and 398 Ma. Complementary biotite analyses reveal a larger spread of ages, but mostly overlap with the white mica ages. Together with previously published dates, our new data constrain rapid MCC exhumation until *c.* 398 Ma, whereas the Southern WGR away from the detachments was exhumed slightly later (*c.* 393 Ma).

On a larger scale, the available dates from different geochronometers show large overlaps. The youngest ages in distinct parts of the WGR, however, show significant differences: Southern WGR, *c.* 393 Ma (MCCs *c.* 398 Ma); Central WGR, *c.* 375 Ma; and Northern WGR, *c.* 390 Ma. They constrain variable durations of ductile behaviour, correlating to the volume of ductile rocks in each segment. Chronological breaks coincide with metamorphic discontinuities across sinistral transfer zones and low-angle detachments (hinterland- and/or foreland-directed). To explain the structural, metamorphic and chronological segmentation of the WGR, we consider rheological contrasts in the overthickened crust during collapse: (1) across the strike of the orogen (foreland v. hinterland); (2) between different segments of the infrastructure; and (3) between the infrastructure and the orogenic wedge. Non-uniform transtensional crustal stretching dragged out distinct crustal levels below the detachments and became progressively dominated by sinistral transfer zones. The suggested model highlights the role of transfer zones in continental extensional systems and the highly variable effects of orogenic collapse on the lithosphere.

Acknowledgements We are grateful for thorough reviews by Fernando Corfu, Chris Mark and Editor Stephen Daly, which improved the presentation of our data and the clarity of our arguments. A previous version of this paper benefited from constructive and critical comments by Clare Warren, Uwe Ring, Jeff Lee, Bradley Hacker and an anonymous reviewer. Irina Dumitru and Irene Heggstad at UiB helped with sample preparation and imaging. We thank Martin Whitehouse, Kerstin Lindén, Heejin Jeon and Gavin Kenny at Nordsim Stockholm for facilitating the U–Pb zircon analyses. Nordsim contribution number 668.

Author contributions **JDW**: conceptualization (lead), data curation (lead), formal analysis (lead), funding acquisition (lead), investigation (lead), visualization (lead), writing – original draft (lead), writing – review and editing (lead); **JJ**: formal analysis (equal), funding acquisition (equal), investigation (equal), project administration (lead), supervision (lead), validation (equal), writing – original draft (supporting), writing – review and editing (supporting); **HF**: formal analysis (supporting), funding acquisition (supporting), supervision (equal), validation (equal), visualization (supporting), writing – original draft (supporting), writing – review and editing (supporting); **MG**: data curation (equal), formal analysis (equal), methodology (equal), writing – original draft (supporting), writing – review and editing (supporting); **PTO**: funding acquisition (supporting), supervision (supporting), validation (supporting), writing – original draft (supporting), writing – review and editing (supporting).

Funding This work was funded by the VISTA, a basic research programme in collaboration between The Norwegian Academy of Science and Letters and Equinor (grant number 6271).

Data availability All data generated or analysed during this study are included in this published article and the Supplementary Material.

Scientific editing by Stephen Daly

References

Andersen, T.B. 1998. Extensional tectonics in the Caledonides of southern Norway, an overview. *Tectonophysics*, **285**, 333–351, https://doi.org/10.1016/S0040-1951(97)00277-1

Andersen, T.B. and Jansen, O.J. 1987. The Sunnhordland Batholith, W Norway – regional setting and internal structure, with emphasis on the Granitoid Plutons. *Norsk Geologisk Tidsskrift*, **67**, 159–183.

Andersen, T.B. and Jamtveit, B. 1990. Uplift of deep crust during orogenic extensional collapse – a model based on field studies in the Sogn-Sunnfjord region of Western Norway. *Tectonics*, **9**, 1097–1111, https://doi.org/10.1029/TC009i005p01097

Andersen, T.B., Jamtveit, B., Dewey, J.F. and Swensson, E. 1991. Subduction and eduction of continental-crust – major mechanisms during continent–continent collision and orogenic extensional collapse, a model based on the South Norwegian Caledonides. *Terra Nova*, **3**, 303–310, https://doi.org/10.1111/j.1365-3121.1991.tb00148.x

Andersen, T.B., Osmundsen, P.T. and Jolivet, L. 1994. Deep crustal fabrics and a model for the extensional collapse of the southwest Norwegian Caledonides. *Journal of Structural Geology*, **16**, 1191–1203, https://doi.org/10.1016/0191-8141(94)90063-9

Andersen, T.B., Berry, H.N., Lux, D.R. and Andresen, A. 1998. The tectonic significance of pre-Scandian $^{40}Ar/^{39}Ar$ phengite cooling ages in the Caledonides of western Norway. *Journal of the Geological Society, London*, **155**, 297–309, https://doi.org/10.1144/gsjgs.155.2.0297

Andersen, T.B., Torsvik, T.H., Eide, E.A., Osmundsen, P.T. and Faleide, J.I. 1999. Permian and Mesozoic extensional faulting within the Caledonides of central south Norway. *Journal of the Geological Society, London*, **156**, 1073–1080, https://doi.org/10.1144/gsjgs.156.6.1073

Andersen, T.B., Corfu, F., Labrousse, L. and Osmundsen, P.T. 2012. Evidence for hyperextension along the pre-Caledonian margin of Baltica. *Journal of the Geological Society, London*, **169**, 601–612, https://doi.org/10.1144/0016-76492012-011

Austrheim, H. 1987. Eclogitization of lower crustal granulites by fluid migration through shear zones. *Earth and Planetary Science Letters*, **81**, 221–232, https://doi.org/10.1016/0012-821X(87)90158-0

Bingen, B. and Solli, A. 2009. Geochronology of magmatism in the Caledonian and Sveconorwegian belts of Baltica: synopsis for detrital zircon provenance studies. *Norwegian Journal of Geology*, **89**, 267–290.

Bingen, B., Austrheim, H., Whitehouse, M.J. and Davis, W.J. 2004. Trace element signature and U–Pb geochronology of eclogite-facies zircon, Bergen Arcs, Caledonides of W Norway. *Contributions to Mineralogy and Petrology*, **147**, 671–683, https://doi.org/10.1007/s00410-004-0585-z

Bingen, B., Skar, O. *et al.* 2005. Timing of continental building in the Sveconorwegian orogen, SW Scandinavia. *Norwegian Journal of Geology*, **85**, 87–116.

Bingen, B., Nordgulen, O. and Viola, G. 2008. A four-phase model for the Sveconorwegian orogeny, SW Scandinavia. *Norwegian Journal of Geology*, **88**, 43–72.

Boundy, T.M., Essene, E.J., Hall, C.M., Austrheim, H. and Halliday, A.N. 1996. Rapid exhumation of lower crust during continent–continent collision and late extension: evidence from Ar-40/Ar-39 incremental heating of hornblendes and muscovites, Caledonian orogen, western Norway. *GSA Bulletin*, **108**, 1425–1437, https://doi.org/10.1130/0016-7606(1996)108<1425:REOLCD>2.3.CO;2

Braathen, A., Nordgulen, O., Osmundsen, P.T., Andersen, T.B., Solli, A. and Roberts, D. 2000. Devonian, orogen-parallel, opposed extension in the Central Norwegian Caledonides. *Geology*, **28**, 615–618, https://doi.org/10.1130/0091-7613(2000)28<615:DOOEIT>2.0.CO;2

Braathen, A., Osmundsen, P.T., Nordgulen, Ø., Roberts, D. and Meyer, G.B. 2002. Orogen-parallel extension of the Caledonides in northern Central Norway: an overview. *Norwegian Journal of Geology*, **82**, 225–241.

Braathen, A., Osmundsen, P.T. and Gabrielsen, R.H. 2004. Dynamic development of fault rocks in a crustal-scale detachment: an example from western Norway. *Tectonics*, **23**, 1–21, https://doi.org/10.1029/2003tc001558

Braathen, A., Osmundsen, P.T., Maher, H. and Ganerød, M. 2018. The Keisarhjelmen detachment records Silurian–Devonian extensional collapse in Northern Svalbard. *Terra Nova*, **30**, 34–39, https://doi.org/10.1111/ter.12305

Brueckner, H.K. 2018. The great eclogite debate of the Western Gneiss Region, Norwegian Caledonides: the in situ crustal v. exotic mantle origin controversy. *Journal of Metamorphic Geology*, **36**, 517–527, https://doi.org/10.1111/jmg.12314

Brueckner, H.K. and Cuthbert, S.J. 2013. Extension, disruption, and translation of an orogenic wedge by exhumation of large ultrahigh-pressure terranes: examples from the Norwegian Caledonides. *Lithosphere*, **5**, 277–289, https://doi.org/10.1130/L256.1

Butler, J.P., Beaumont, C. and Jamieson, R.A. 2015. Paradigm lost: buoyancy thwarted by the strength of the Western Gneiss Region (ultra) high-pressure terrane, Norway. *Lithosphere*, **7**, 379–407, https://doi.org/10.1130/L426.1

Butler, J.P., Jamieson, R.A., Dunning, G.R., Pecha, M.E., Robinson, P. and Steenkamp, H.M. 2018. Timing of metamorphism and exhumation in the Nordøyane ultra-high-pressure domain, Western Gneiss Region, Norway: new constraints from complementary CA-ID-TIMS and LA-MC-ICP-MS geochronology. *Lithos*, **310–311**, 153–170, https://doi.org/10.1016/j.lithos.2018.04.006

Camacho, A., Lee, J.K.W. *et al.* 2012. Planar defects as Ar traps in trioctahedral micas: a mechanism for increased Ar retentivity in phlogopite. *Earth and Planetary Science Letters*, **341–344**, 255–267, https://doi.org/10.1016/j.epsl.2012.05.041

Cao, S. and Neubauer, F. 2016. Deep crustal expressions of exhumed strike-slip fault systems: shear zone initiation on rheological boundaries. *Earth-Science Reviews*, **162**, 155–176, https://doi.org/10.1016/j.earscirev.2016.09.010

Chauvet, A. and Dallmeyer, R.D. 1992. $^{40}Ar/^{39}Ar$ mineral dates related to Devonian extension in the southwestern Scandinavian Caledonides. *Tectonophysics*, **210**, 155–177, https://doi.org/10.1016/0040-1951(92)90133-Q

Chauvet, A. and Seranne, M. 1994. Extension-parallel folding in the Scandinavian Caledonides – implications for late-orogenic processes. *Tectonophysics*, **238**, 31–54, https://doi.org/10.1016/0040-1951(94)90048-5

Christiansson, P., Faleide, J.I. and Berge, A.M. 2000. Crustal structure in the northern North Sea: an integrated geophysical study. *Geological Society, London, Special Publications*, **167**, 15–40, https://doi.org/10.1144/gsl.Sp.2000.167.01.02

Coint, N., Slagstad, T., Roberts, N.M.W., Marker, M., Rohr, T. and Sorensen, B.E. 2015. The Late Mesoproterozoic Sirdal magmatic belt, SW Norway: relationships between magmatism and metamorphism and implications for Sveconorwegian orogenesis. *Precambrian Research*, **265**, 57–77, https://doi.org/10.1016/j.precamres.2015.05.002

Corfu, F., Hanchar, J.M., Hoskin, P.W. and Kinny, P. 2003. Atlas of zircon textures. *Reviews in Mineralogy and Geochemistry*, **53**, 469–500, https://doi.org/10.2113/0530469

Corfu, F., Andersen, T. and Gasser, D. 2014. The Scandinavian Caledonides: main features, conceptual advances and critical questions. *Geological Society, London, Special Publications*, **390**, 9–43, https://doi.org/10.1144/SP390.25

Cuthbert, S.J., Carswell, D.A., Krogh-Ravna, E.J. and Wain, A. 2000. Eclogites and eclogites in the Western Gneiss Region, Norwegian Caledonides. *Lithos*, **52**, 165–195, https://doi.org/10.1016/S0024-4937(99)00090-0

Cutts, J.A., Smit, M.A., Kooijman, E. and Schmitt, M. 2019. Two-stage cooling and exhumation of deeply subducted continents. *Tectonics*, **38**, 863–877, https://doi.org/10.1029/2018tc005292

Dallmeyer, R.D. 1990. $^{40}Ar/^{39}Ar$ mineral age record of a polyorogenic evolution within the Seve and Köli nappes, Trøndelag, Norway. *Tectonophysics*, **179**, 199–226, https://doi.org/10.1016/0040-1951(90)90291-F

Dallmeyer, R.D., Johannson, L. and Möller, C. 1992. Chronology of Caledonian high-pressure granulite-facies metamorphism, uplift, and deformation within northern parts of the Western Gneiss Region, Norway. *GSA Bulletin*, **104**, 444–455, https://doi.org/10.1130/0016-7606(1992)104<0444:Cochpg>2.3.Co;2

Denèle, Y., Roques, D., Ganne, J., Chardon, D., Rousse, S. and Barbey, P. 2017. Strike-slip metamorphic core complexes: gneiss domes emplaced in releasing bends. *Geology*, **45**, 903–906, https://doi.org/10.1130/g39065.1

Dewey, J.F. 2002. Transtension in arcs and orogens. *International Geology Review*, **44**, 402–439, https://doi.org/10.2747/0020-6814.44.5.402

Dewey, J.F. and Strachan, R.A. 2003. Changing Silurian–Devonian relative plate motion in the Caledonides: sinistral transpression to sinistral transtension. *Journal of the Geological Society, London*, **160**, 219–229, https://doi.org/10.1144/0016-764902-085

Di Vincenzo, G., Viti, C. and Rocchi, S. 2003. The effect of chlorite interlayering on $^{40}Ar–^{39}Ar$ biotite dating: an $^{40}Ar–^{39}Ar$ laser-probe and TEM investigation of variably chloritised biotites. *Contributions to Mineralogy and Petrology*, **145**, 643–658, https://doi.org/10.1007/s00410-003-0472-z

Duretz, T., Gerya, T.V., Kaus, B.J.P. and Andersen, T.B. 2012. Thermomechanical modeling of slab eduction. *Journal of Geophysical Research: Solid Earth*, **117**, 1–21, https://doi.org/10.1029/2012jb009137

Eide, E.A., Torsvik, T.H. and Andersen, T.B. 1997. Absolute dating of brittle fault movements: late Permian and late Jurassic extensional fault breccias in western Norway. *Terra Nova*, **9**, 135–139, https://doi.org/10.1046/j.1365-3121.1997.d01-21.x

Eide, E.A., Haabesland, N.E., Osmundsen, P.T., Andersen, T.B., Roberts, D. and Kendrick, M.A. 2005. Modern techniques and Old Red problems – determining the age of continental sedimentary deposits with Ar-40/Ar-39 provenance analysis in west-central Norway. *Norwegian Journal of Geology*, **85**, 133–149.

Engvik, A.K., Willemoes-Wissing, B. and Lutro, O. 2018. High-temperature, decompressional equilibration of the eclogite facies orogenic root (Western Gneiss Region, Norway). *Journal of Metamorphic Geology*, **36**, 529–545, https://doi.org/10.1111/jmg.12418

Eskola, P.E. 1948. The problem of mantled gneiss domes. *Quarterly Journal of the Geological Society, London*, **104**, 461–476, https://doi.org/10.1144/gsl.jgs.1948.104.01-04.21

Fauconnier, J., Labrousse, L., Andersen, T.B., Beyssac, O., Duprat-Oualid, S. and Yamato, P. 2014. Thermal structure of a major crustal shear zone, the basal thrust in the Scandinavian Caledonides. *Earth and Planetary Science Letters*, **385**, 162–171, https://doi.org/10.1016/j.epsl.2013.10.038

Fazlikhani, H., Fossen, H., Gawthorpe, R.L., Faleide, J.I. and Bell, R.E. 2017. Basement structure and its influence on the structural configuration of the northern North Sea rift. *Tectonics*, **36**, 1151–1177, https://doi.org/10.1002/2017TC004514

Fossen, H. 1989. Geology of the Minor Bergen Arc, West Norway. *Norges Geologiske Undersøkelse Bulletin*, **416**, 47–62.

Fossen, H. 1992. The role of extensional tectonics in the Caledonides of south Norway. *Journal of Structural Geology*, **14**, 1033–1046, https://doi.org/10.1016/0191-8141(92)90034-T

Fossen, H. 1993. Linear fabrics in the Bergsdalen Nappes, southwest Norway – implications for deformation history and fold development. *Norsk Geologisk Tidsskrift*, **73**, 95–108.

Fossen, H. 2000. Extensional tectonics in the Caledonides: synorogenic or postorogenic? *Tectonics*, **19**, 213–224, https://doi.org/10.1029/1999tc900066

Fossen, H. 2010. Extensional tectonics in the North Atlantic Caledonides: a regional view. *Geological Society, London, Special Publications*, **335**, 767–793, https://doi.org/10.1144/SP335.31

Fossen, H. and Rykkelid, E. 1992. Postcollisional extension of the Caledonide Orogen in Scandinavia – structural expressions and tectonic significance. *Geology*, **20**, 737–740, https://doi.org/10.1130/0091-7613(1992)020<0737:Peotco>2.3.Co;2

Fossen, H. and Dallmeyer, R.D. 1998. Ar-40/Ar-39 muscovite dates from the nappe region of southwestern Norway: dating extensional deformation in the Scandinavian Caledonides. *Tectonophysics*, **285**, 119–133, https://doi.org/10.1016/S0040-1951(97)00187-X

Fossen, H. and Dunlap, W.J. 1998. Timing and kinematics of Caledonian thrusting and extensional collapse, southern Norway: evidence from Ar-40/Ar-39 thermochronology. *Journal of Structural Geology*, **20**, 765–781, https://doi.org/10.1016/S0191-8141(98)00007-8

Fossen, H. and Dunlap, W.J. 1999. On the age and tectonic significance of Permo-Triassic dikes in the Bergen–Sunnhordland region, southwestern Norway. *Norsk Geologisk Tidsskrift*, **79**, 169–178, https://doi.org/10.1080/002919699433807

Fossen, H. and Hurich, C.A. 2005. The Hardangerfjord shear zone in SW Norway and the North Sea: a large-scale low-angle shear zone in the Caledonian crust. *Journal of the Geological Society, London*, **162**, 675–687, https://doi.org/10.1144/0016-764904-136

Fossen, H. and Dunlap, W.J. 2006. Age constraints on the late Caledonian (Scandian) deformation in the major Bergen Arc, SW Norway. *Norwegian Journal of Geology*, **86**, 59–70.

Fossen, H. and Ragnhildstveit, J. 2008. *Berggrunnskart Bergen 1115 I, M 1:50.000*. Norges geologiske undersøkelse.

Fossen, H., Teyssier, C. and Whitney, D.L. 2013. Transtensional folding. *Journal of Structural Geology*, **56**, 89–102, https://doi.org/10.1016/j.jsg.2013.09.004

Fossen, H., Gabrielsen, R.H., Faleide, J.I. and Hurich, C.A. 2014. Crustal stretching in the Scandinavian Caledonides as revealed by deep seismic data. *Geology*, **42**, 791–794, https://doi.org/10.1130/G35842.1

Fossen, H., Fazlikhani, H., Faleide, J.I., Ksienzyk, A.K. and Dunlap, W.J. 2016. Post-Caledonian extension in the West Norway–northern North Sea region: the role of structural inheritance. *Geological Society, London, Special Publications*, **439**, 465–486, https://doi.org/10.1144/SP439.6 https://doi.org/10.1144/SP439.6

Fossen, H., Cavalcante, G.C. and de Almeida, R.P. 2017. Hot versus cold orogenic behavior: comparing the Araçuai–West Congo and the Caledonian Orogens. *Tectonics*, **36**, 2159–2178, https://doi.org/10.1002/2017TC004743

Gabrielsen, R.H., Faleide, J.I., Pascal, C., Braathen, A., Nystuen, J.P., Etzelmuller, B. and O'Donnell, S. 2010. Latest Caledonian to Present tectonomorphological development of southern Norway. *Marine and Petroleum Geology*, **27**, 709–723, https://doi.org/10.1016/j.marpetgeo.2009.06.004

Gee, D.G., Fossen, H., Henriksen, N. and Higgins, A.K. 2008. From the early Paleozoic platforms of Baltica and Laurentia to the Caledonide orogen of Scandinavia and Greenland. *Episodes*, **31**, 44–51, https://doi.org/10.18814/epiiugs/2008/v31i1/007

Gee, D.G., Juhlin, C., Pascal, C. and Robinson, P. 2010. Collisional orogeny in the Scandinavian Caledonides (COSC). *GFF*, **132**, 29–44, https://doi.org/10.1080/11035891003759188

Gerya, T. 2010. Dynamical instability produces transform faults at mid-ocean ridges. *Science*, **329**, 1047–1050, https://doi.org/10.1126/science.1191349

Gessner, K., Gallardo, L.A., Markwitz, V., Ring, U. and Thomson, S.N. 2013. What caused the denudation of the Menderes Massif: review of crustal evolution, lithosphere structure, and dynamic topography in southwest Turkey. *Gondwana Research*, **24**, 243–274, https://doi.org/10.1016/j.gr.2013.01.005

Gordon, S.M., Whitney, D.L., Teyssier, C. and Fossen, H. 2013. U–Pb dates and trace-element geochemistry of zircon from migmatite, Western Gneiss Region, Norway: significance for history of partial melting in continental subduction. *Lithos*, **170**, 35–53, https://doi.org/10.1016/j.lithos.2013.02.003

Gordon, S.M., Whitney, D.L., Teyssier, C., Fossen, H. and Kylander-Clark, A. 2016. Geochronology and geochemistry of zircon from the northern Western Gneiss Region: insights into the Caledonian tectonic history of western Norway. *Lithos*, **246–247**, 134–148, https://doi.org/10.1016/j.lithos.2015.11.036

Griffin, W.L. and Brueckner, H.K. 1980. Caledonian Sm–Nd ages and a crustal origin for Norwegian eclogites. *Nature*, **285**, 319–321, https://doi.org/10.1038/285319a0

Hacker, B.R. and Gans, P.B. 2005. Continental collisions and the creation of ultrahigh-pressure terranes: petrology and thermochronology of nappes in the central Scandinavian Caledonides. *GSA Bulletin*, **117**, 117–134, https://doi.org/10.1130/B25549.1

Hacker, B.R., Andersen, T.B., Root, D.B., Mehl, L., Mattinson, J.M. and Wooden, J.L. 2003. Exhumation of high-pressure rocks beneath the Solund Basin, Western Gneiss Region of Norway. *Journal of Metamorphic Geology*, **21**, 613–629, https://doi.org/10.1046/j.1525-1314.2003.00468.x

Hacker, B.R., Andersen, T.B., Johnston, S., Kylander-Clark, A.R.C., Peterman, E.M., Walsh, E.O. and Young, D. 2010. High-temperature deformation during continental-margin subduction and exhumation: the ultrahigh-pressure Western Gneiss Region of Norway. *Tectonophysics*, **480**, 149–171, https://doi.org/10.1016/j.tecto.2009.08.012

Hacker, B.R., Kylander-Clark, A.R.C., Holder, R., Andersen, T.B., Peterman, E.M., Walsh, E.O. and Munnikhuis, J.K. 2015. Monazite response to ultrahigh-pressure subduction from U–Pb dating by laser ablation split stream. *Chemical Geology*, **409**, 28–41, https://doi.org/10.1016/j.chemgeo.2015.05.008

Hartz, E.H., Martin, M.W., Andresen, A. and Andersen, T.B. 2002. Volcanic rocks in the Devonian Solund Basin, Western Norway: large landslides of Silurian (439 Ma) rhyolites. *Journal of the Geological Society, London*, **159**, 121–128, https://doi.org/10.1144/0016-764901-063

Hirth, G. and Tullis, J. 1992. Dislocation creep regimes in quartz aggregates. *Journal of Structural Geology*, **14**, 145–159, https://doi.org/10.1016/0191-8141(92)90053-Y

Hossack, J.R. 1984. The geometry of listric growth faults in the Devonian basins of Sunnfjord, W Norway. *Journal of the Geological Society, London*, **141**, 629–637, https://doi.org/10.1144/gsjgs.141.4.0629

Huet, B., Le Pourhiet, L., Labrousse, L., Burov, E. and Jolivet, L. 2011. Post-orogenic extension and metamorphic core complexes in a heterogeneous crust: the role of crustal layering inherited from collision. Application to the Cyclades (Aegean domain). *Geophysical Journal International*, **184**, 611–625, https://doi.org/10.1111/j.1365-246X.2010.04849.x

Jakob, J., Andersen, T.B. and Kjøll, H.J. 2019. A review and reinterpretation of the architecture of the south and south-central Scandinavian Caledonides—a magma-poor to magma-rich transition and the significance of the reactivation of rift inherited structures. *Earth-Science Reviews*, **192**, 513–528, https://doi.org/10.1016/j.earscirev.2019.01.004

Jeon, H. and Whitehouse, M.J. 2015. A critical evaluation of U–Pb calibration schemes used in SIMS zircon geochronology. *Geostandards and Geoanalytical Research*, **39**, 443–452, https://doi.org/10.1111/j.1751-908X.2014.00325.x

Johansson, L., Schöberg, H. and Solyom, Z., 1993. The age and regional correlation of the Svecofennian Geitfjell granite, Vestranden, Norway. *Norwegian Journal of Geology*, **73**, 133–143.

Johnston, S., Hacker, B.R. and Ducea, M.N. 2007*a*. Exhumation of ultrahigh-pressure rocks beneath the Hornelen segment of the Nordfjord–Sogn detachment zone, western Norway. *GSA Bulletin*, **119**, 1232–1248, https://doi.org/10.1130/B26172.1

Johnston, S.M., Hacker, B.R. and Andersen, T.B. 2007*b*. Exhuming Norwegian ultrahigh-pressure rocks: overprinting extensional structures and the role of the Nordfjord–Sogn detachment zone. *Tectonics*, **26**, 1–12, https://doi.org/doi:10.1029/2005TC001933

Jolivet, L., Raimbourg, H., Labrousse, L., Avigad, D., Leroy, Y., Austrheim, H. and Andersen, T.B. 2005. Softening triggered by eclogitization, the first step toward exhumation during continental subduction. *Earth and Planetary Science Letters*, **237**, 532–547, https://doi.org/10.1016/j.epsl.2005.06.047

Keay, S., Lister, G. and Buick, I. 2001. The timing of partial melting, Barrovian metamorphism and granite intrusion in the Naxos metamorphic core complex, Cyclades, Aegean Sea, Greece. *Tectonophysics*, **342**, 275–312, https://doi.org/10.1016/S0040-1951(01)00168-8

Kendrick, M.A., Eide, E.A., Roberts, D. and Osmundsen, P.T. 2004. The Middle to Late Devonian Høybakken detachment, central Norway: ^{40}Ar–^{39}Ar evidence for prolonged late/post-Scandian extension and uplift. *Geological Magazine*, **141**, 329–344, https://doi.org/10.1017/s0016756803008811

Kjøll, H.J., Andersen, T.B., Corfu, F., Labrousse, L., Tegner, C., Abdelmalak, M.M. and Planke, S. 2019. Timing of breakup and thermal evolution of a pre-Caledonian Neoproterozoic exhumed magma-rich rifted margin. *Tectonics*, **38**, 1843–1862, https://doi.org/10.1029/2018TC005375

Kohn, M.J., Corrie, S.L. and Markley, C. 2015. The fall and rise of metamorphic zircon. *American Mineralogist*, **100**, 897–908, https://doi.org/10.2138/am-2015-5064

Kolderup, C.F. and Kolderup, N.H. 1940. *Geology of the Bergen Arc System*. Bergen Museum, Bergen.

Krabbendam, M. and Dewey, J.F. 1998. Exhumation of UHP rocks by transtension in the Western Gneiss Region, Scandinavian Caledonides. *Geological Society, London, Special Publications*, **135**, 159–181, https://doi.org/10.1144/GSL.SP.1998.135.01.11

Krill, A. 1985. Relationships between the Western Gneiss Region and the Trondheim Region – stockwerk-tectonics reconsidered. *In*: Gee, D.G. and Sturt, B.A. (eds) *The Caledonide Orogen – Scandinavia and Related Areas*. Wiley, 475–483.

Krogh, T.E., Kamo, S.L., Robinson, P., Terry, M.P. and Kwok, K. 2011. U–Pb zircon geochronology of eclogites from the Scandian Orogen, northern Western Gneiss Region, Norway: 14–20 million years between eclogite crystallization and return to amphibolite-facies conditions. *Canadian Journal of Earth Sciences*, **48**, 441–472, https://doi.org/10.1139/E10-076

Ksienzyk, A.K., Dunkl, I., Jacobs, J., Fossen, H. and Kohlmann, F. 2014. From orogen to passive margin: constraints from fission track and (U–Th)/He analyses on Mesozoic uplift and fault reactivation in SW Norway. *Geological Society, London, Special Publications*, **390**, 679–702, https://doi.org/10.1144/SP390.27

Ksienzyk, A.K., Wemmer, K. *et al.* 2016. Post-Caledonian brittle deformation in the Bergen area, West Norway: results from K–Ar illite fault gouge dating. *Norwegian Journal of Geology*, **96**, 275–299, https://doi.org/10.17850/njg96-3-06

Kuhn, A., Glodny, J., Austrheim, H. and Raheim, A. 2002. The Caledonian tectono-metamorphic evolution of the Lindas Nappe: constraints from U–Pb, Sm-Nd and Rb-Sr ages of granitoid dykes. *Norwegian Journal of Geology*, **82**, 45–57.

Kylander-Clark, A.R.C. and Hacker, B.R. 2014. Age and significance of felsic dikes from the UHP western gneiss region. *Tectonics*, **33**, 2342–2360, https://doi.org/10.1002/2014TC003582

Kylander-Clark, A.R.C., Hacker, B.R. and Mattinson, J.M. 2008. Slow exhumation of UHP terranes: titanite and rutile ages of the Western Gneiss

Region, Norway. *Earth and Planetary Science Letters*, **272**, 531–540, https://doi.org/10.1016/j.epsl.2008.05.019

Labrousse, L., Jolivet, L., Agard, P., Hebert, R. and Andersen, T.B. 2002. Crustal-scale boudinage and migmatization of gneiss during their exhumation in the UHP province of Western Norway. *Terra Nova*, **14**, 263–270, https://doi.org/10.1046/j.1365-3121.2002.00422.x

Labrousse, L., Jolivet, L., Andersen, T., Agard, P., Hébert, R., Maluski, H. and Schärer, U. 2004. Pressure–temperature–time deformation history of the exhumation of ultra-high pressure rocks in the Western Gneiss Region, Norway. *Geological Society of America, Special Papers*, **380**, 155–183, https://doi.org/10.1130/0-8137-2380-9.155

Labrousse, L., Hetényi, G., Raimbourg, H., Jolivet, L. and Andersen, T.B. 2010. Initiation of crustal-scale thrusts triggered by metamorphic reactions at depth: insights from a comparison between the Himalayas and Scandinavian Caledonides. *Tectonics*, **29**, 1–14, https://doi.org/10.1029/2009tc002602

Labrousse, L., Prouteau, G. and Ganzhorn, A.-C. 2011. Continental exhumation triggered by partial melting at ultrahigh pressure. *Geology*, **39**, 1171–1174, https://doi.org/10.1130/g32316.1

Labrousse, L., Huet, B., Le Pourhiet, L., Jolivet, L. and Burov, E. 2016. Rheological implications of extensional detachments: Mediterranean and numerical insights. *Earth-Science Reviews*, **161**, 233–258, https://doi.org/10.1016/j.earscirev.2016.09.003

Larsen, O., Fossen, H., Langeland, K. and Pedersen, R.B. 2003. Kinematics and timing of polyphase post-Caledonian deformation in the Bergen area, SW Norway. *Norwegian Journal of Geology*, **83**, 149–165.

Le Pourhiet, L., Huet, B., May, D.A., Labrousse, L. and Jolivet, L. 2012. Kinematic interpretation of the 3D shapes of metamorphic core complexes. *Geochemistry, Geophysics, Geosystems*, **13**, 1–17, https://doi.org/10.1029/2012GC004271

Ludwig, K.R. 1998. On the treatment of concordant uranium–ead ages. *Geochimica et Cosmochimica Acta*, **62**, 665–676, https://doi.org/10.1016/S0016-7037(98)00059-3

Ludwig, K.R. 2003. *User's Manual for Isoplot 3.00: A Geochronological Toolkit for Microsoft Excel*. Kenneth R. Ludwig.

McClay, K.R., Norton, M.G., Coney, P. and Davis, G.H. 1986. Collapse of the Caledonian orogen and the Old Red Sandstone. *Nature*, **323**, 147–149, https://doi.org/10.1038/323147a0

McDonald, C.S., Warren, C.J., Mark, D.F., Halton, A.M., Kelley, S.P. and Sherlock, S.C. 2016. Argon redistribution during a metamorphic cycle: consequences for determining cooling rates. *Chemical Geology*, **443**, 182–197, https://doi.org/10.1016/j.chemgeo.2016.09.028

Milnes, A.G. and Koyi, H.A. 2000. Ductile rebound of an orogenic root: case study and numerical model of gravity tectonics in the Western Gneiss Complex, Caledonides, southern Norway. *Terra Nova*, **12**, 1–7, https://doi.org/10.1046/j.1365-3121.2000.00266.x

Milnes, A., Wennberg, O., Skår, Ø. and Koestler, A. 1997. Contraction, extension and timing in the South Norwegian Caledonides: the Sognefjord transect. *Geological Society, London, Special Publications*, **121**, 123–148, https://doi.org/10.1144/GSL.SP.1997.121.01.06

Norton, M.G. 1986. Late Caledonide extension in Western Norway – a response to extreme crustal thickening. *Tectonics*, **5**, 195–204, https://doi.org/10.1029/TC005i002p00195

Norton, M.G. 1987. The Nordfjord–Sogn detachment, W Norway. *Norsk Geologisk Tidsskrift*, **67**, 93–106.

Osmundsen, P.T. and Andersen, T.B. 1994. Caledonian compressional and late-orogenic extensional deformation in the Staveneset area, Sunnfjord, Western Norway. *Journal of Structural Geology*, **16**, 1385–1401, https://doi.org/10.1016/0191-8141(94)90004-3

Osmundsen, P.T. and Andersen, T.B. 2001. The middle Devonian basins of western Norway: sedimentary response to large-scale transtensional tectonics? *Tectonophysics*, **332**, 51–68, https://doi.org/10.1016/S0040-1951(00)00249-3

Osmundsen, P.T., Braathen, A., Nordgulen, Ø., Roberts, D., Meyer, G.B. and Eide, E. 2003. The Devonian Nesna shear zone and adjacent gneiss-cored culminations, north–central Norwegian Caledonides. *Journal of the Geological Society, London*, **160**, 137–150, https://doi.org/10.1144/0016-764901-173

Osmundsen, P.T., Braathen, A. *et al.* 2005. Metamorphic core complexes and gneiss-cored culminations along the Mid-Norwegian margin: an overview and some current ideas. *Norwegian Petroleum Society, Special Publications*, **12**, 29–41, https://doi.org/10.1016/S0928-8937(05)80042-6

Osmundsen, P.T., Eide, E.A. *et al.* 2006. Kinematics of the Høybakken detachment zone and the Møre–Trøndelag fault complex, central Norway. *Journal of the Geological Society, London*, **163**, 303–318, https://doi.org/10.1144/0016-764904-129

Pedersen, V.K., Huismans, R.S. and Moucha, R. 2016. Isostatic and dynamic support of high topography on a North Atlantic passive margin. *Earth and Planetary Science Letters*, **446**, 1–9, https://doi.org/10.1016/j.epsl.2016.04.019

Peron-Pinvidic, G. and Osmundsen, P.T. 2020. From orogeny to rifting: insights from the Norwegian 'reactivation phase'. *Scientific Reports*, **10**, 14860, https://doi.org/10.1038/s41598-020-71893-z

Platt, J.P., Behr, W.M. and Cooper, F.J. 2015. Metamorphic core complexes: windows into the mechanics and rheology of the crust. *Journal of the Geological Society, London,* **172**, 9–27, https://doi.org/10.1144/jgs2014-036

Ragnhildstveit, J. and Helliksen, D. 1997. *Geologisk kart over Norge, berggrunnskart Bergen – M 1:250.000*, Norges geologiske undersøkelse.

Rey, P., Burg, J.-P. and Casey, M. 1997. The Scandinavian Caledonides and their relationship to the Variscan belt. *Geological Society, London, Special Publications*, **121**, 179–200, https://doi.org/10.1144/gsl.sp.1997.121.01.08

Rey, P., Vanderhaeghe, O. and Teyssier, C. 2001. Gravitational collapse of the continental crust: definition, regimes and modes. *Tectonophysics*, **342**, 435–449, https://doi.org/10.1016/S0040-1951(01)00174-3

Roberts, D. 2003. The Scandinavian Caledonides: event chronology, palaeogeographic settings and likely, modern analogues. *Tectonophysics*, **365**, 283–299, https://doi.org/10.1016/S0040-1951(03)00026-X

Roberts, N.M.W. and Slagstad, T. 2015. Continental growth and reworking on the edge of the Columbia and Rodinia supercontinents; 1.86–0.9 Ga accretionary orogeny in southwest Fennoscandia. *International Geology Review*, **57**, 1582–1606, https://doi.org/10.1080/00206814.2014.958579

Robinson, P. 1995. Extension of Trollheimen tectono-stratigraphic sequence in deep synclines near Molde and Brativag, Western Gneiss Region, southern Norway. *Norsk Geologisk Tidsskrift*, **75**, 181–197.

Robinson, P., Roberts, D., Gee, D.G. and Solli, A. 2014. A major synmetamorphic Early Devonian thrust and extensional fault system in the Mid-Norway Caledonides: relevance to exhumation of HP and UHP rocks. *Geological Society, London, Special Publications*, **390**, 241–270, https://doi.org/10.1144/sp390.24

Røhr, T.S., Corfu, F., Austrheim, H. and Andersen, T.B. 2004. Sveconorwegian U–Pb zircon and monazite ages of granulite-facies rocks, Hisarøya, Gulen, Western Gneiss Region, Norway. *Norwegian Journal of Geology*, **84**, 251–256.

Røhr, T.S., Bingen, B., Robinson, P. and Reddy, S.M. 2013. Geochronology of Paleoproterozoic augen gneisses in the Western Gneiss Region, Norway: evidence for Sveconorwegian zircon neocrystallization and Caledonian zircon deformation. *Journal of Geology*, **121**, 105–128, https://doi.org/10.1086/669229

Root, D. and Corfu, F. 2012. U–Pb geochronology of two discrete Ordovician high-pressure metamorphic events in the Seve Nappe Complex, Scandinavian Caledonides. *Contributions to Mineralogy and Petrology*, **163**, 769–788, https://doi.org/10.1007/s00410-011-0698-0

Root, D.B., Hacker, B.R., Gans, P.B., Ducea, M.N., Eide, E.A. and Mosenfelder, J.L. 2005. Discrete ultrahigh-pressure domains in the Western Gneiss Region, Norway: implications for formation and exhumation. *Journal of Metamorphic Geology*, **23**, 45–61, https://doi.org/10.1111/j.1525-1314.2005.00561.x

Rosenberg, C.L. and Handy, M.R. 2005. Experimental deformation of partially melted granite revisited: implications for the continental crust. *Journal of Metamorphic Geology*, **23**, 19–28, https://doi.org/10.1111/j.1525-1314.2005.00555.x

Schneider, J., Bosch, D. and Monié, P. 2008. Individualization of textural and reactional microdomains in eclogites from the Bergen Arcs (Norway): consequences for Rb/Sr and Ar/Ar radiochronometer behavior during polymetamorphism. *Geochemistry, Geophysics, Geosystems*, **9**, 1–28, https://doi.org/10.1029/2008GC002098

Schouenborg, B.E., Johansson, L. and Gorbatschev, R., 1991. U/Pb zircon ages of basement gneisses and discordant felsic dykes from Vestranden, westernmost Baltic Shield and central Norwegian Caledonides. *Geologische Rundschau*, **80**, 121–134, https://doi.org/10.1007/BF01828771

Séguret, M., Séranne, M., Chauvet, A. and Brunel, A. 1989. Collapse basin: a new type of extensional sedimentary basin from the Devonian of Norway. *Geology*, **17**, 127–130, https://doi.org/10.1130/0091-7613(1989)017<0127:Cbanto>2.3.Co;2

Seranne, M. 1992. Late Palaeozoic kinematics of the Møre–Trøndelag fault zone and adjacent areas, central Norway. *Norsk Geologisk Tidsskrift*, **72**, 141–158.

Seranne, M. and Séguret, M. 1987. The Devonian basins of western Norway: tectonics and kinematics of an extending crust. *Geological Society, London, Special Publications*, **28**, 537–548, https://doi.org/10.1144/GSL.SP.1987.028.01.35

Skår, Ø. and Pedersen, R.B. 2003. Relations between granitoid magmatism and migmatization: U–Pb geochronological evidence from the Western Gneiss Complex, Norway. *Journal of the Geological Society, London*, **160**, 935–946, https://doi.org/10.1144/0016-764901-121

Slagstad, T. and Kirkland, C.L. 2018. Timing of collision initiation and location of the Scandian orogenic suture in the Scandinavian Caledonides. *Terra Nova*, **30**, 179–188, https://doi.org/10.1111/ter.12324

Slagstad, T., Roberts, N.M.W., Marker, M., Rohr, T.S. and Schiellerup, H. 2013. A non-collisional, accretionary Sveconorwegian orogen. *Terra Nova*, **25**, 30–37, https://doi.org/10.1111/ter.12001

Slagstad, T., Roberts, N.M.W. *et al.* 2018. Magma-driven, high-grade metamorphism in the Sveconorwegian Province, southwest Norway, during the terminal stages of Fennoscandian Shield evolution. *Geosphere*, **14**, 861–882, https://doi.org/10.1130/ges01565.1

Souche, A., Beyssac, O. and Andersen, T.B. 2012. Thermal structure of supra-detachment basins: a case study of the Devonian basins of western Norway. *Journal of the Geological Society, London*, **169**, 427–434, https://doi.org/10.1144/0016-76492011-155

Spencer, K.J., Hacker, B.R. *et al.* 2013. Campaign-style titanite U–Pb dating by laser-ablation ICP: implications for crustal flow, phase transformations and titanite closure. *Chemical Geology*, **341**, 84–101, https://doi.org/10.1016/j.chemgeo.2012.11.012

Stacey, J.S. and Kramers, J.D. 1975. Approximation of terrestrial lead isotope evolution by a 2-stage model. *Earth and Planetary Science Letters*, **26**, 207–221, https://doi.org/10.1016/0012-821x(75)90088-6

Steiger, R.H. and Jäger, E. 1977. Subcommission on Geochronology – convention on use of decay constants in geochronology and cosmochronology. *Earth and Planetary Science Letters*, **36**, 359–362, https://doi.org/10.1016/0012-821x(77)90060-7

Streule, M.J., Strachan, R.A., Searle, M.P. and Law, R.D. 2010. Comparing Tibet–Himalayan and Caledonian crustal architecture, evolution and mountain building processes. *Geological Society, London, Special Publications*, **335**, 207–232, https://doi.org/10.1144/sp335.10

Stübner, K., Warren, C., Ratschbacher, L., Sperner, B., Kleeberg, R., Pfänder, J. and Grujic, D. 2017. Anomalously old biotite $^{40}Ar/^{39}Ar$ ages in the NW Himalaya. *Lithosphere*, **9**, 366–383, https://doi.org/10.1130/l586.1

Svensen, H., Jamtveit, B., Banks, D.A. and Karlsen, D. 2001. Fluids and halogens at the diagenetic–metamorphic boundary: evidence from veins in continental basins, western Norway. *Geofluids*, **1**, 53–70, https://doi.org/10.1046/j.1468-8123.2001.11003.x

Templeton, J.A. 2015. *Structural evolution of the Hornelen Basin (Devonian, Norway) from detrital thermochronology*. PhD thesis, Columbia University.

Torsvik, T.H. 2019. Earth history: a journey in time and space from base to top. *Tectonophysics*, **760**, 297–313, https://doi.org/10.1016/j.tecto.2018.09.009

Tucker, R.D., Raheim, A., Krogh, T.E. and Corfu, F. 1987. Uranium–lead zircon and titanite ages from the northern portion of the Western Gneiss Region, south-central Norway. *Earth and Planetary Science Letters*, **81**, 203–211, https://doi.org/10.1016/0012-821x(87)90156-7

Tucker, R., Krogh, T. and Råheim, A. 1990. Proterozoic evolution and age-province boundaries in the central part of the Western Gneiss Region, Norway: results of U–Pb dating of accessory minerals from Trondheimsfjord to Geiranger. *In*: Gower, C.F., *et al.* (eds) *Mid-Proterozoic Laurentia-Baltica*, Geological Association of Canada, St. John's, Canada, **38**, 149–173.

Vanderhaeghe, O. 2012. The thermal–mechanical evolution of crustal orogenic belts at convergent plate boundaries: a reappraisal of the orogenic cycle. *Journal of Geodynamics*, **56–57**, 124–145, https://doi.org/10.1016/j.jog.2011.10.004

Vavra, G., Gebauer, D., Schmid, R. and Compston, W. 1996. Multiple zircon growth and recrystallization during polyphase Late Carboniferous to Triassic metamorphism in granulites of the Ivrea Zone (Southern Alps): an ion microprobe (SHRIMP) study. *Contributions to Mineralogy and Petrology*, **122**, 337–358, https://doi.org/10.1007/s004100050132

Vetti, V.V. and Fossen, H. 2012. Origin of contrasting Devonian supradetachment basin types in the Scandinavian Caledonides. *Geology*, **40**, 571–574, https://doi.org/10.1130/G32512.1

Wain, A. 1997. New evidence for coesite in eclogite and gneisses: defining an ultrahigh-pressure province in the Western Gneiss region of Norway. *Geology*, **25**, 927–930, https://doi.org/10.1130/0091-7613(1997)025<0927:Nefcie>2.3.Co;2

Walczak, K., Cuthbert, S., Kooijman, E., Majka, J. and Smit, M.A. 2019. U–Pb zircon age dating of diamond-bearing gneiss from Fjørtoft reveals repeated burial of the Baltoscandian margin during the Caledonian Orogeny. *Geological Magazine*, **156**, 1949–1964, https://doi.org/10.1017/S0016756819000268

Walsh, E.O., Hacker, B.R., Gans, P.B., Grove, M. and Gehrels, G. 2007. Protolith ages and exhumation histories of (ultra)high-pressure rocks across the Western Gneiss Region, Norway. *GSA Bulletin*, **119**, 289–301, https://doi.org/https://doi.org/10.1130/B25817.1

Walsh, E.O., Hacker, B.R., Gans, P.B., Wong, M.S. and Andersen, T.B. 2013. Crustal exhumation of the Western Gneiss Region UHP terrane, Norway: $^{40}Ar/^{39}Ar$ thermochronology and fault-slip analysis. *Tectonophysics*, **608**, 1159–1179, https://doi.org/10.1016/j.tecto.2013.06.030

Warren, C.J. 2013. Exhumation of (ultra-)high-pressure terranes: concepts and mechanisms. *Solid Earth*, **4**, 75–92, https://doi.org/10.5194/se-4-75-2013

Warren, C.J., Kelley, S.P., Sherlock, S.C. and McDonald, C.S. 2012. Metamorphic rocks seek meaningful cooling rate: interpreting $^{40}Ar/^{39}Ar$ ages in an exhumed ultra-high-pressure terrane. *Lithos*, **155**, 30–48, https://doi.org/10.1016/j.lithos.2012.08.011

Wennberg, O.P., Milnes, A.G. and Winsvold, I. 1998. The northern Bergen Arc shear zone – an oblique-lateral ramp in the Devonian extensional detachment system of western Norway. *Norsk Geologisk Tidsskrift*, **78**, 169–184.

White, L.T. and Ireland, T.R. 2012. High-uranium matrix effect in zircon and its implications for SHRIMP U–Pb age determinations. *Chemical Geology*, **306–307**, 78–91, https://doi.org/10.1016/j.chemgeo.2012.02.025

Whitehouse, M.J. and Kamber, B.S. 2005. Assigning dates to thin gneissic veins in high-grade metamorphic terranes: a cautionary tale from Akilia, southwest Greenland. *Journal of Petrology*, **46**, 291–318, https://doi.org/10.1093/petrology/egh075

Whitehouse, M.J., Claesson, S., Sunde, T. and Vestin, J. 1997. Ion microprobe U–Pb zircon geochronology and correlation of Archaean gneisses from the Lewisian Complex of Gruinard Bay, northwestern Scotland. *Geochimica et Cosmochimica Acta*, **61**, 4429–4438, https://doi.org/10.1016/S0016-7037(97)00251-2

Whitehouse, M.J., Kamber, B.S. and Moorbath, S. 1999. Age significance of U-Th-Pb zircon data from early Archaean rocks of west Greenland – a reassessment based on combined ion-microprobe and imaging studies. *Chemical Geology*, **160**, 201–224, https://doi.org/10.1016/S0009-2541(99)00066-2

Wiedenbeck, M., Alle, P. *et al.* 1995. Three natural zircon standards for U-Th-Pb, Lu-Hf, trace element and REE analyses. *Geostandards Newsletter*, **19**, 1–23, https://doi.org/10.1111/j.1751-908X.1995.tb00147.x

Wiest, J.D., Jacobs, J., Ksienzyk, A.K. and Fossen, H. 2018. Sveconorwegian vs. Caledonian orogenesis in the eastern Øygarden Complex, SW Norway – geochronology, structural constraints and tectonic implications. *Precambrian Research*, **305**, 1–18, https://doi.org/10.1016/j.precamres.2017.11.020

Wiest, J.D., Osmundsen, P.T., Jacobs, J. and Fossen, H. 2019. Deep crustal flow within post-orogenic metamorphic core complexes – insights from the southern Western Gneiss Region of Norway. *Tectonics*, **38**, 4267–4289, https://doi.org/10.1029/2019TC005708

Wiest, J.D., Fossen, H. and Jacobs, J. 2020*a*. Shear zone evolution during core complex exhumation – implications for continental detachments. *Journal of Structural Geology*, **140**, 104139, https://doi.org/10.1016/j.jsg.2020.104139

Wiest, J.D., Wrona, T., Bauck, M.S., Fossen, H., Gawthorpe, R.L., Osmundsen, P.T. and Faleide, J.I. 2020*b*. From Caledonian collapse to North Sea Rift: the extended history of a metamorphic core complex. *Tectonics*, **39**, e2020TC006178, https://doi.org/10.1029/2020tc006178

Young, D.J. 2017. Structure of the (ultra)high-pressure Western Gneiss Region, Norway: imbrication during Caledonian continental margin subduction. *GSA Bulletin*, **130**, 926–940, https://doi.org/10.1130/b31764.1

Young, D.J. and Kylander-Clark, A.R.C. 2015. Does continental crust transform during eclogite facies metamorphism? *Journal of Metamorphic Geology*, **33**, 331–357, https://doi.org/doi:10.1111/jmg.12123

Young, D.J., Hacker, B.R., Andersen, T.B. and Gans, P.B. 2011. Structure and $^{40}Ar/^{39}Ar$ thermochronology of an ultrahigh-pressure transition in western Norway. *Journal of the Geological Society, London*, **168**, 887–898, https://doi.org/10.1144/0016-76492010-075